J. Fluid Mech. (2004), *vol.* 515, *pp.* 99–133.
DOI: 10.1017/S0022112004000618 Printed in the United Kingdom

Influence of mean loading on noise generated by the interaction of gusts with a cascade: downstream radiation

By N. PEAKE[1] AND E. J. KERSCHEN[2]

[1]Department of Applied Mathematics and Theoretical Physics, University of Cambridge, Wilberforce Road, Cambridge CB3 0WA, UK

[2]Department of Aerospace & Mechanical Engineering, University of Arizona, Tucson, AZ 85721, USA

(Received 27 June 2002 and in revised form 23 June 2004)

We consider the effects of blade mean loading on the noise generated by the interaction between convected vorticity and a blade row. The blades are treated as flat plates aligned at a non-zero incidence angle, δ, to the oncoming stream, and we take harmonic components of the incident vorticity field with reduced frequency k, and use asymptotic analysis in the realistic limit $k \gg 1$, $\delta \ll 1$ with $k\delta = O(1)$. In a previous paper (Peake & Kerschen, *J. Fluid Mech.*, vol. 347 (1997), pp. 315–346) we have analysed the sound radiated back upstream, but the field in the blade passages and the sound radiated downstream are also of considerable practical interest, and are considered in this paper. The flow is seen to consist of inner regions around each leading edge, in which sound is generated by the local gust–airfoil and gust–flow interactions, and an outer region in which the incident gust and the acoustic radiation interact with the non-uniform mean flow and the other blades. It is shown that the complicated multiple interactions between the blades can be represented by images in potential–streamfunction space, yielding closed-form expressions for the phase distortion experienced by sound waves propagating down the blade passages. The acoustic radiation downstream of the cascade at $O(1)$ distances is dominated by the duct-mode beams that emanate from the passages, while the far downstream field is generated by the diffraction of the duct modes by the trailing edges. The modal amplitudes of the radiation field far downstream tend to be largest when the mode direction is close to the propagation direction of the duct mode which generated it, corresponding to the way (in uniform flow) in which the radiation from a single blade passage tends to be beamed in the duct-mode directions. Although the diffraction coefficient for the scattering from a single trailing edge is singular in these directions, we show how uniformly valid expressions can be derived by combining the trailing-edge fields in an appropriate way, thereby describing the larger amplitude in the beam directions. The steady non-uniform flow downstream has the effect of tilting the directions of the beams by $O(\delta)$ angles away from the duct-mode directions, which are explicitly determined. Throughout this analysis it will be seen that the interaction with the non-uniform mean flow introduces phase corrections of size $O(k\delta)$, which, given the way in which interference effects between the multiple blades dominate unsteady cascade flow, proves to be highly significant.

1. Introduction

In Peake & Kerschen (1997, hereafter referred to as (I)), we considered the interaction between convected vortical gusts of reduced frequency k and a cascade of zero-thickness flat plates aligned at an angle δ to the oncoming flow. Using asymptotic analysis in the limits $k \gg 1, \delta \ll 1$ with $k\delta = O(1)$, we investigated the acoustic field radiated upstream of the cascade. It turns out that in this asymptotic limit the unsteady flow consists of inner regions around each leading edge scaling on the gust wavelength, in which sound is generated by the interaction between the steady flow and the gust, and by the blocking of the gust momentum by the blade. In the outer region away from the leading edges the incident gust and the radiation are distorted by their interaction with the mean flow. It is therefore shown in (I) that the upstream radiation can be thought of as being generated by effective point sources located at each leading edge, with directivity patterns that are a function of the radiation angle (see Myers & Kerschen 1995, 1997). The way in which the radiation from these sources propagates to the upstream observer, either directly or via diffraction or reflection by other blades, is fully described in (I). However, no consideration was given in (I) to the effects of the mean loading on the field downstream of the cascade leading edges, either for the field in the blade passages or for the field downstream of the trailing edges. In this paper we therefore aim to extend (I) by considering these two areas, and it will be seen that while sound is still only generated near the leading edges, the interaction of the unsteady field with the blades and the trailing edges will be considerably more complicated than in the case of the upstream radiation.

A review of earlier work in this area has been given in (I), and we need not repeat that here. We note, however, that extensive numerical calculations of the unsteady lift and downstream radiation have been completed, both in terms of solution of the full compressible Euler equations (see Verdon 1993) and in terms of solution of Goldstein's (1978) rapid distortion equations (e.g. Atassi, Subramaniam & Scott 1990; Abdelhamid & Atassi 2000). Our approach here, however, is different in that we aim to combine previous analytical and asymptotic work; in effect, the analysis presented here and in (I) combines analysis of cascades in uniform flow (e.g. Koch 1971; Peake 1992, 1993) with that of isolated airfoils in non-uniform flow (e.g. Myers & Kerschen 1995).

In § 2 and § 3 we describe the mathematical formulation of the problem and summarize those results from (I) which are required in the present study. In the first instance we use potential–streamfunction coordinates aligned with the flow at upstream infinity, and this proves particularly convenient since the cascade in physical space is then mapped onto a cascade of straight-line segments in the new space as well, and the gust is convected along lines of constant ψ. The effective sources located at each leading edge produce sound waves which propagate downstream, potentially undergoing multiple reflections by adjacent blades. In § 4 we show how this field can be represented by an array of image sources, which yield a family of downstream-propagating duct modes. When $\delta = 0$ these waves form the familiar set of simple duct modes, but for $\delta \neq 0$ it will be seen that quite considerable phase variations are induced by the non-uniform mean flow.

In § 5 and § 6 we consider the flow downstream of the cascade. In all the foregoing analysis it has proved convenient to use coordinates aligned with the mean flow at upstream infinity, but for the radiation downstream it is preferable to make a transformation to coordinates aligned with the mean flow at downstream infinity. In physical space this means simply rotating the coordinate axes through the cascade turning angle, but the transformation between the corresponding potential–streamfunction spaces is more complicated, given that the difference between the

upstream and downstream steady flow speeds and densities, and the effect of the mean circulation round each blade, must be included.

The field at $O(1)$ distances downstream of the cascade is dominated by the duct-mode beams, with the scattering by the trailing edges introducing only secondary terms of relative order $O(k^{-1/2})$. Fresnel regions lie along the edges of the beams, and these gradually spread to encompass the full widths of the beams at downstream distances of $O(k)$.

In contrast to the near downstream field, the far downstream field is dominated by the scattering of the duct modes by the trailing edges. We convert the infinite set of scattered cylindrical waves to a finite sum over the cut-on radiation modes for the downstream region. In the far downstream field, the main effects of the mean loading appear as a modification of the effective cascade geometry in potential–streamfunction space. The inclination of the blades to the downstream flow is $O(\delta)$; however in typical cases it is numerically smaller than δ, and it follows that the additional phase distortion experienced by the radiation as it propagates downstream from the cascade has a less-marked effect than that found upstream of the cascade. The radiation that exits the back of the cascade, however, has been strongly influenced by mean loading effects. One particular feature of the far downstream radiation is that the modal amplitudes tend to be largest when the modal propagation direction is close to the 'propagation direction' of one of the duct modes. In uniform flow, the far-field radiation from a given blade passage is beamed in these duct-mode directions, and we show explicitly how the non-uniform mean flow has the effect of tilting these directions by an $O(\delta)$ amount.

2. Mathematical formulation

The system under consideration and the mathematical formulation are fully described in (I), and we provide only a brief description here. We consider an infinite cascade of zero-thickness flat plates of length $2b_*$ (the suffix $*$ denotes physical quantities). The cascade stagger angle and leading-edge separation are α_* and Δ_* respectively, and we write $d_* = \Delta_* \cos\alpha_*$, $s_* = \Delta_* \sin\alpha_*$; see figure 1. The blades are labelled $n = 0, \pm1, \pm2, \ldots$, with the origin located at the leading edge of blade 0. The mean flow far upstream has a uniform, subsonic speed U_∞ and is aligned at a non-zero angle-of-attack δ to the blades. We non-dimensionalize lengths by b_*, time by b_*/U_∞ and pressures by $\rho_\infty U_\infty^2$, with ρ_∞ the density at upstream infinity. We define the upstream mean-flow Mach number $M_\infty = U_\infty/c_\infty$, with c_∞ the upstream speed of sound, and consider only the subsonic case $M_\infty < 1$.

In order to simplify subsequent analysis, we shall make a change of variables from the physical x_*–y_* space into ϕ–ψ space, where ϕ and ψ are the normalized potential and streamfunction of the steady flow:

$$\phi = \frac{\phi_*}{U_\infty b_*}, \quad \psi = \frac{\beta_\infty \psi_*}{U_\infty b_*}. \tag{2.1}$$

The factor $\beta_\infty = (1 - M_\infty^2)^{1/2}$ in the definition of ψ corresponds to a Prandtl–Glauert transformation. The physical cascade maps onto a cascade in ϕ–ψ space (see figure 2) with stagger angle α and leading-edge separation Δ, where

$$\alpha = \tan^{-1}[\beta_\infty \tan(\alpha_* - \delta)], \tag{2.2}$$

$$\Delta = \Delta_* (\cos^2(\alpha_* - \delta) + \beta_\infty^2 \sin^2(\alpha_* - \delta))^{1/2}/b_*, \tag{2.3}$$

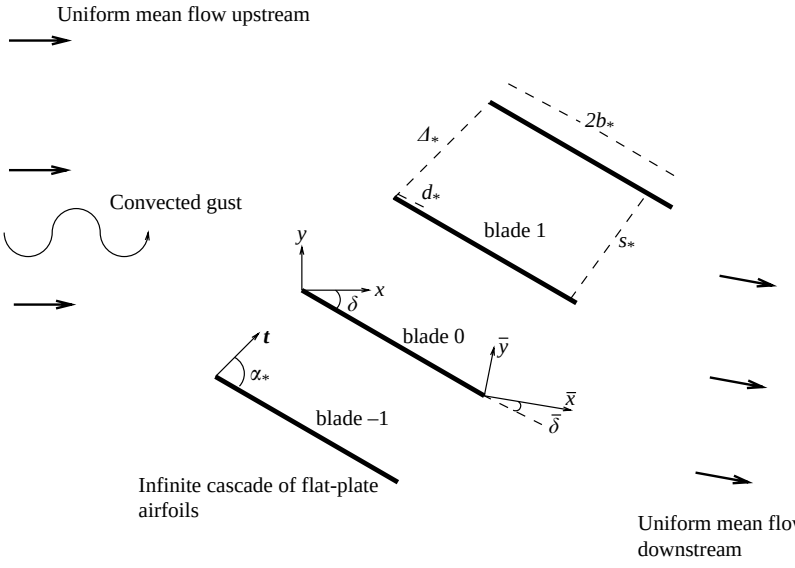

FIGURE 1. The cascade geometry in physical space. The x_*–y_* and $\bar{x}_*$–$\bar{y}_*$ axes are aligned with the mean flow at upstream and downstream infinity respectively, and the acute angles between the blades and the x_*- and $\bar{x}_*$-axes are δ and $\bar{\delta}$.

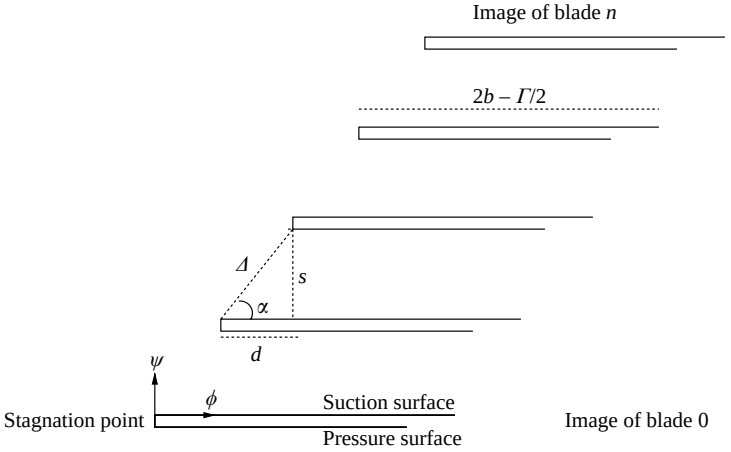

FIGURE 2. The cascade geometry in ϕ–ψ space.

and we set $d = \Delta\cos\alpha$, $s = \Delta\sin\alpha$. Note that the stagger angle α in ϕ–ψ space is determined by the angle of the upstream flow relative to a line parallel to the front face of the cascade. The arbitrary constants in ϕ and ψ are chosen such that $\phi = \psi = 0$ at the leading edge of blade zero in ϕ–ψ space. (This is the image of the stagnation point for blade zero in physical space.) Due to the non-zero circulation round each blade, the upper and lower surfaces of the trailing edge of blade zero are mapped onto two different points in ϕ–ψ space, $\phi = l^{\pm} \equiv 2b \mp \Gamma/2$; this point must be accounted for when we consider scattering by the cascade trailing edges. Here $2b = 2 + O(\delta)$ is the mean chord length in ϕ–ψ space, and $U_\infty b_* \Gamma (< 0)$ is the mean circulation around the blade. The numerical values of b and Γ for given cascade parameters are determined using conformal mapping, as discussed below.

We then require a description for the mean flow as a function of ϕ and ψ. The required quantities are the normalized flow speed and the flow angle. Since we suppose that $\delta \ll 1$, the steady flow through the cascade can be determined using thin-airfoil theory. A Prandtl–Glauert transformation then reduces the compressible flow to an equivalent incompressible flow, so that the mean flow can be determined using conformal mapping; full details are given in Robinson & Laurmann (1956) and in (I). The $O(\delta)$ mean flow perturbation can then be expressed in terms of a complex potential F and we have

$$\zeta = \zeta_0 + \delta F(\zeta_0), \tag{2.4}$$

where $\zeta = \phi + \mathrm{i}\psi$, $\zeta_0 = \phi_0 + \mathrm{i}\psi_0 = (x_* + \mathrm{i}\beta_\infty y_*)/b_*$, and the free constant in F is chosen such that $F(0) = 0$. Then, since $\zeta = \zeta_0 + O(\delta)$, the mean flow perturbation is given by

$$q - \mathrm{i}\mu = \frac{\mathrm{d}F(\zeta)}{\mathrm{d}\zeta}, \tag{2.5}$$

where the normalized flow speed is $U_*/U_\infty = 1 + \delta q$ and the flow angle is $\delta\beta_\infty\mu$.

From the geometry and (2.5) it is clear that the boundary condition on the blade surfaces is

$$\frac{\partial \mathrm{Im}[F]}{\partial \phi} = \frac{1}{\beta_\infty}. \tag{2.6}$$

(This implies that the effective incidence angle of the blades in Prandtl–Glauert space is δ/β_∞.) The boundary condition can be integrated to give the value of $\mathrm{Im}[F]$ on blade n in the form

$$\mathrm{Im}[F] = \frac{(\phi - nd)}{\beta_\infty}, \tag{2.7}$$

and we will use this result repeatedly in our subsequent analysis.

We will be concerned with the interaction between the cascade and convected vortical and entropic disturbances, and for definiteness we consider single-frequency harmonic gusts, so that the unsteady velocity fluctuation associated with the gust takes the form far upstream

$$\boldsymbol{v}' = \epsilon U_\infty (A_t, A_n, A_z) \exp(\mathrm{i}k[\phi + k_n\psi + k_z z - t]) \quad \text{as} \quad \phi \to -\infty, \tag{2.8}$$

where k is the gust reduced frequency ($k = \omega_* b_*/U_\infty$, where ω_* is the gust temporal frequency) and the amplitude $\epsilon \ll 1$. A similar representation holds for the entropy disturbance s'.

When considered as a function of physical position, the gust obeys the quasi-periodic condition

$$\boldsymbol{v}'(\boldsymbol{x}_* + \Delta_* \boldsymbol{t}, t) = \exp(\mathrm{i}\sigma)\boldsymbol{v}'(\boldsymbol{x}_*, t), \tag{2.9}$$

where $\boldsymbol{t}$ is the unit vector tangent to the front face of the cascade and the inter-blade phase angle is $\sigma = k(d + k_n s)$. Given the linearity of the problem and the periodicity of the blade geometry in the $\boldsymbol{t}$-direction, it follows that the unsteady field generated by the interaction between the gust and the cascade must also obey (2.9) throughout the fluid, both upstream and downstream of the cascade.

The gust vorticity and entropy are convected and distorted by the non-uniform mean flow according to rapid distortion theory (Goldstein 1978). Kerschen & Balsa (1981) have derived an analytical expression for the distorted forms of $\boldsymbol{v}'$ and s' in this $\delta \ll 1$ limit in terms of the drift. Once the gust reaches the cascade, however, an additional unsteady (irrotational) field is generated by the blocking of the gust momentum by the rigid blade surfaces, and by the interaction of the gust with the

mean-flow gradients. This unsteady irrotational flow can be described in terms of the velocity potential

$$\epsilon U_\infty b_* h(\phi, \psi) \exp(\mathrm{i}k[k_z z - t - M_\infty^2 \phi/\beta_\infty^2]) \exp(\delta M_\infty^2 q), \tag{2.10}$$

where $h(\phi, \psi)$ is termed the modified potential and δq is the perturbation in the mean-flow speed produced by the cascade. Since we will take $k\delta = O(1)$, it follows that the divergence of the drift associated with convection towards the leading-edge stagnation point, which occurs in a region of size $O(\delta^2)$ around the stagnation point, does not affect the leading-order expansion of the unsteady field.

An equation for $h(\phi, \psi)$ has been derived by Kerschen & Myers (1986) in the form

$$(\nabla^2 + k^2 w^2 + \delta \mathscr{L}_1)(h) = \delta k S(\phi, \psi) \exp(\mathrm{i}k\Omega), \tag{2.11}$$

where

$$w^2 = (M_\infty/\beta_\infty^2)^2 - (k_z/\beta_\infty)^2. \tag{2.12}$$

The operator $\mathscr{L}_1$ accounts for refraction of sound by the non-uniform flow, and is given by

$$\mathscr{L}_1(h) = (\gamma + 1) M_\infty^4 \beta_\infty^{-2} \left\{ q \left[\frac{\partial^2 h}{\partial \psi^2} + 2\mathrm{i}k\beta_\infty^{-2} \frac{\partial h}{\partial \phi} + k^2 (w^2 + \beta_\infty^{-4}) \right] - \frac{\partial q}{\partial \phi} \left[\frac{\partial h}{\partial \phi} - \mathrm{i}k\beta_\infty^{-2} h \right] \right\} - 2k^2 w^2 \beta_\infty^2 q h, \tag{2.13}$$

where γ is the ratio of specific heats. The source term $S(\phi, \psi) \exp(\mathrm{i}k\Omega)$ in (2.11) corresponds to the interaction between the gust and the local mean-flow gradients – see equation (2.5) of Myers & Kerschen (1995).

When $k \gg 1$ the mean flow varies slowly on the gust wavelength scale, except in local regions of size $O(k^{-1})$ surrounding each leading edge. The primary sound generation is concentrated in these local leading-edge regions (see § 3). Outside these local regions, the source term $S(\phi, \psi) \exp(\mathrm{i}k\Omega)$ and the boundary condition on the blade surfaces generate only particular solutions that are not related to the sound field – see equations (3.28) and (3.29) of Myers & Kerschen (1995). The sound field is a complementary outer solution of (2.11) which satisfies the no-penetration boundary condition on the airfoil surfaces,

$$\frac{\partial h}{\partial \psi} + \delta M_\infty^2 \frac{\partial q}{\partial \psi} h = 0. \tag{2.14}$$

For our flat-plate airfoils we have $\partial \mu / \partial \phi = 0$ on the blade surfaces. Then, applying the Cauchy–Riemann equations to $F(\zeta)$ we can see that $\partial q / \partial \psi = 0$, so that the exact boundary condition on the blade surfaces is simply

$$\frac{\partial h}{\partial \psi} = 0. \tag{2.15}$$

This result will also be used throughout our subsequent analysis.

Finally, in what follows we will need to calculate the unsteady pressure

$$\epsilon \rho_\infty U_\infty^2 p(\phi, \psi) \exp(\mathrm{i}k[k_z z - t]), \tag{2.16}$$

and this pressure is given in terms of the modified unsteady velocity potential by

$$p = \left[\mathrm{i} \frac{k}{\beta_\infty^2} h - \frac{\partial h}{\partial \phi} \right] \exp(-\mathrm{i}k M_\infty^2 \phi / \beta_\infty^2). \tag{2.17}$$

3. Leading-edge fields

In this section we simply summarize those results from Myers & Kerschen (1995) and (I) which will be required later.

For $k \gg 1$, the sound generation is concentrated in local regions of size $O(k^{-1})$ surrounding each leading edge. In each local region, sound is generated by blocking of the gust velocity by the blade surface, and by the volume source distribution $S(\phi, \psi)\exp(\mathrm{i}k\Omega)$. Note that the lengthscales of the mean flow and the gust become comparable in these local leading-edge regions, so that the gust is distorted 'rapidly' leading to efficient sound generation. Sound is generated by both the unsteady force distribution on the blade surface and the Reynolds' stress fluctuations in the local leading-edge region. Vorticity distortion plays an important role in both sound generation mechanisms. This interaction is essentially equivalent to the isolated-blade problem analysed by Myers & Kerschen (1995).

Outside the local leading-edge regions, the gust distortion is 'slow' and is therefore an inefficient sound generation mechanism. Thus, the sound field in the outer region is a complementary solution of (2.11). The determination of the radiated sound then reduces to a problem in the theory of matched asymptotic expansions, with inner regions around each leading edge and an outer region comprising the rest of space. Matching of the outer region with each leading edge produces an outgoing radiation field with modified velocity potential of the form

$$\frac{D(\theta_n)}{k^{3/2} r_n^{1/2}} \exp(\mathrm{i}kwr_n + \mathrm{i}k\delta P(r_n, \theta_n) + \mathrm{i}n\sigma' + \mathrm{i}k\delta g_l). \tag{3.1}$$

Here, (r_n, θ_n) are polar coordinates in ϕ–ψ space centred on the leading edge of blade n with $0 \leqslant \theta_n < 2\pi$, and the modified inter-blade phase angle is $\sigma' = \sigma + kM_\infty^2 d/\beta_\infty^2$. The quantity $k\delta g_l$ is the drift experienced by the gust in convecting from upstream infinity to the leading edge, and the phase distortion term $k\delta P(r_n, \theta_n)$ corresponds to the refraction experienced by the radiation as it propagates away from the leading edge through the non-uniform steady flow. We have $\delta P(r_n, \theta_n) = V(\theta_n) Q(r_n, \theta_n)$, where

$$V(\theta) = -\beta_\infty^2 w + \frac{(\gamma+1)M_\infty^4}{2\beta_\infty^2 w}(\beta_\infty^{-2} - w\cos\theta)^2, \tag{3.2}$$

and

$$Q(r_n, \theta_n) = \mathrm{Re}\{\exp(-\mathrm{i}\theta_n)[\delta F(r_n \exp(\mathrm{i}\theta_n))]\}. \tag{3.3}$$

The directivity $D(\theta) = D_0(\theta) + \delta k^{1/2} D_1(\theta)$ is given in Myers & Kerschen (1995) and in (I). We can see from (3.1) that non-zero mean loading acts to introduce a significant $O(k\delta)$ phase change into the field radiated from each leading edge, as well as modifying the directivity – the directivity $D(\theta)$ is the zero-mean-loading result $D_0(\theta)$, plus a correction of size $O(\delta k^{1/2})$.

Once the radiation described by (3.1) has been emitted from each leading-edge region, it will potentially undergo a complicated interaction with the other blades in the cascade before reaching the observer in the far field upstream. In fact, it is shown in (I) that the radiation reaching the upstream observer contains four components:

(i) the direct field, which propagates from each leading edge directly to the observer without interacting with any other blades;

(ii) two rays from a given leading edge propagate in opposite directions along the front face of the cascade, and are rescattered by each of the other leading edges before reaching the observer;

(iii) one ray from a given leading edge is reflected by the blade immediately below, and is then rescattered by the leading edge from which it originated before reaching the observer, and this process continues indefinitely;

(iv) in the case of a staggered cascade, the radiation corresponding to the first three contributions can also reach the observer via a single reflection off the lower blade.

It is also shown in (I) that other contributions, such as rescattering of radiation from the leading edges by the trailing edges, can be neglected in calculating the upstream radiation to the asymptotic order in k and δ considered, so that (i)–(iv) provide the leading-order approximation to the upstream radiation. In short, the upstream radiation is generated by an effective acoustic source located at each blade leading edge (contributions i–iii), together with the radiation from the image of this source in the lower blade (contribution iv).

In this paper, we are concerned with extending these results to calculate the unsteady field in the passages between the blades and downstream of the cascade. In order to do this we must first consider the radiation which emanates from each leading edge in the downstream direction, which will subsequently be multiply reflected by the adjacent blades and scattered by the trailing edges. It was shown in (I) that the radiation emanating from the leading edge of blade n (i.e. contributions i–iii above) has unsteady velocity potential

$$f(\phi^n, \psi^n) \equiv \frac{g(\theta_n)}{r_n^{1/2}} \exp(\mathrm{i}kwr_n + \mathrm{i}k\delta P(r_n, \theta_n) + \mathrm{i}n\sigma'), \tag{3.4}$$

where

$$g(\theta_n) = k^{-3/2}\left\{D(\theta_n)\exp(\mathrm{i}k\delta g_l) - \frac{\mathrm{i}B^1 w\sin\alpha}{k^{1/2}} D_0(\theta_n, w\cos\alpha) + \frac{\mathrm{i}wB^2\sin\alpha}{k^{1/2}} D_0(\theta_n, -w\cos\alpha) + \frac{\mathrm{i}wB^3}{k^{1/2}} D_0(\theta_n, 0)\right\} \tag{3.5}$$

with

$$\left.\begin{aligned} B^1 &= \sum_{m=1}^{\infty}\left\{\frac{D(\pi+\alpha)\exp(\mathrm{i}kwm\Delta + \mathrm{i}m\sigma' + \mathrm{i}k\delta g_l)}{m^{3/2}\Delta^{1/2}}\right\},\\ B^2 &= \sum_{m=1}^{\infty}\left\{\frac{D(\alpha)\exp(\mathrm{i}kwm\Delta - \mathrm{i}m\sigma' + \mathrm{i}k\delta g_l)}{m^{3/2}\Delta^{1/2}}\right\},\\ B^3 &= \sum_{m=1}^{\infty}\left\{\frac{D(3\pi/2)\exp(2\mathrm{i}kwms + \mathrm{i}k\delta mp_2 + \mathrm{i}k\delta g_l)}{m^{3/2}(2s)^{1/2}}\right\}, \end{aligned}\right\} \tag{3.6}$$

and where ϕ^n, ψ^n are centred on the leading edge of blade n. In (3.5), the first term $D(\theta)$ corresponds to the direct field which propagates to the point (r_n, θ_n) (contribution i), the terms $B^{1,2}$ correspond to the radiation which first emanated from the leading edges of blades $n \pm 1, n \pm 2, \ldots$ respectively, before being rescattered by leading edge n (contribution ii), and the term B^3 corresponds to the radiation emitted from the leading edge of blade n and repeatedly re-reflected by blade $n-1$ (contribution iii). The quantity $k\delta p_2$ in B^3 is the net phase distortion (due to the mean-flow perturbation) experienced by the radiation in a single bounce from blade n to blade $n-1$ and back; an expression for p_2 is given in (I). It turns out that the mean flow perturbation induces no net phase distortion for radiation propagating from one leading edge to the next, so that no such terms appear in $B^{1,2}$. We note

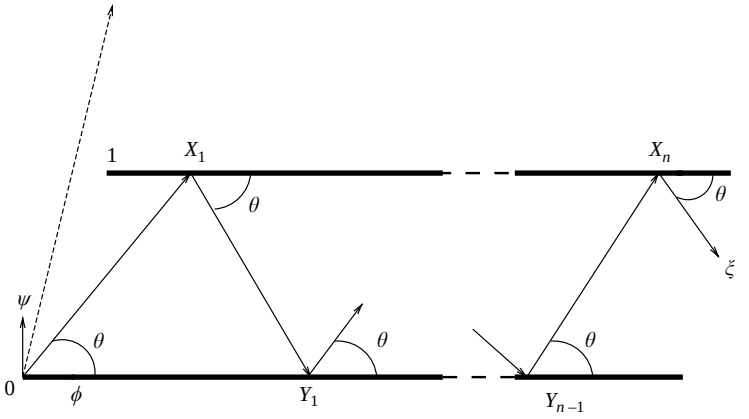

FIGURE 3. Schematic diagram of a typical ray path in ϕ–ψ space undergoing multiple reflections between blades 0 and 1. Note how the dotted ray from leading edge 0 is not reflected by blade 1.

that the full form of the directivity, $D(\theta)$, is required in the first term in (3.5), while in the remaining terms, which are $O(k^{-1/2})$ smaller, only the simpler zero-mean-loading directivity $D_0(\theta)$ is required to the asymptotic order considered.

4. The cut-on duct modes between the blades

We now proceed to determine the downstream-propagating field between adjacent blades, which originates from the effective sources at the leading edges as described in the previous section.

4.1. *Image sources*

For definiteness we consider the passage between blades 0 and 1, with the field in other passages being given by the quasi-periodicity condition (2.9). As has already been described, sound is generated at the leading edges of blades 0 and 1, and will then propagate downstream between the blades. We consider an observer at the point (ϕ, ψ) located in the blade passage, and note that sound from the leading edges will reach the observer not only directly but also via multiple reflections off the two rigid blades. The situation is described schematically in figure 3. There is an infinite number of possible ray paths from the leading edge of blade 1 to the observer, involving an arbitrarily large number of bounces between the blades, while only a finite number of such paths can reach the observer from leading edge 0 (thanks to the cascade stagger, rays from leading edge 0 which leave at a sufficiently oblique angle are not reflected by blade 1).

The reflected fields will be represented by an array of image sources above and below the blades, exactly in parallel to the work of Yee, Felsen & Keller (1968), who used the method of images to describe the reflection of incident duct modes at the end of a waveguide (see also Jones 1994 for a description of related problems). There are two issues to consider here: first the location of the image sources, and second the phase distortion experienced by the sound as it propagates along the bouncing rays. The location of the image sources is straightforward. Boundary condition (2.15) shows that the source at the leading edge of blade 0 has an image source in blade 1 located at $(0, 2s)$, which will in turn have an image in blade 0 located at $(0, -2s)$. This sequence of images continues indefinitely, but as has already been argued the observer

will receive radiation from only a finite number of them due to the cascade stagger. The image fields associated with the source at leading edge 1 can be constructed in exactly the same way, and this time the observer will receive contributions from all the image sources.

The second issue to consider is the phase distortion along the bouncing ray directions. The phase distortion appears in the coordinate transformation $(x, y) \to (\phi, \psi)$, and in the influence of the operator $\mathscr{L}_1$ in (2.11). Since $\delta \ll 1$, the leading-order ray paths in ϕ–ψ space are simply straight lines, and the phase distortion due to $\mathscr{L}_1$ is then obtained by integrating along the leading-order ray paths, say from point ζ_a to ζ_b, leading to the expression (Myers & Kerschen 1995)

$$k\delta P(\zeta_b, \zeta_a) = k\delta V(\theta)\mathrm{Re}\{\exp(-\mathrm{i}\theta)[F(\zeta_b) - F(\zeta_a)]\}, \tag{4.1}$$

where θ is the angle between the line segment from ζ_a to ζ_b and the positive ϕ-direction. Consider first radiation which is emitted from the leading edge of blade 0, and which propagates to the point $\zeta = \phi + \mathrm{i}\psi$ in ϕ–ψ space, having first been reflected n times by blade 1 and $n-1$ times by blade 0. This reflected field can be represented by an image source located above the blade passage in ϕ–ψ space at the point $\zeta_n = \mathrm{i}2ns$, and the ray that reaches the end point ζ then makes an angle $-\theta$ with the ϕ-axis, where $\theta = \tan^{-1}[(2ns - \psi)/\phi]$. The complete ray path from the leading edge of blade 0 to the downstream point ζ can be split into a series of segments in the ϕ–ψ plane as shown in figure 3, where the angles of the segments alternate in sign. In order to determine the total phase distortion experienced by the radiation in travelling from the leading edge of blade 0 to the point ζ along this path, we simply add up the phase distortion along each line segment, and using (4.1) together with the fact that $V(\theta) = V(-\theta)$, it follows that this phase distortion becomes

$$\begin{aligned} kV(\theta)\mathrm{Re}\{&\exp(-\mathrm{i}\theta)[\delta F(X_1) - \delta F(0)] + \exp(\mathrm{i}\theta)[\delta F(Y_1) - \delta F(X_1)] + \ldots \\ &+ \ldots + \exp(-\mathrm{i}\theta)[\delta F(X_n) - \delta F(Y_{n-1})] + \exp(\mathrm{i}\theta)[\delta F(\zeta) - \delta F(X_n)]\}, \end{aligned} \tag{4.2}$$

where the points X_i, Y_i are shown in figure 3. Collecting terms involving $\delta F(X_i)$ and $\delta F(Y_i)$, it turns out that we need only the imaginary parts of these quantities, which can be found from (2.7) as

$$\left.\begin{aligned} \mathrm{Im}\{\delta F(X_i)\} &= \frac{(2i-1)s\delta}{\beta_\infty \tan\theta} - d\delta/\beta_\infty + O(\delta^2), \quad i = 1, 2, \ldots n, \\ \mathrm{Im}\{\delta F(Y_i)\} &= \frac{2is\delta}{\beta_\infty \tan\theta} + O(\delta^2), \qquad\qquad\quad i = 1, 2, \ldots n-1. \end{aligned}\right\} \tag{4.3}$$

The total phase distortion experienced in travelling from the leading edge of blade 0 to the observer point along the path shown in figure 3 is denoted $\wp_2$, and using (4.2) and (4.3) we find

$$\wp_2 = k\delta V(\theta)\left[\frac{2n\Delta}{\beta_\infty}\sin(\alpha - \theta) + \mathrm{Re}\{\exp(\mathrm{i}\theta)F(\zeta)\}\right]. \tag{4.4}$$

The phase distortion, $\wp_1$, experienced by a wave emitted from leading edge 0 which is reflected n times by both blade 0 and blade 1, is calculated similarly. The relevant image source in this case is located below the blade passage at $\zeta_n = -\mathrm{i}2ns$, and the ray angle is $\theta = \tan^{-1}[(2ns + \psi)/\phi]$. We then obtain

$$\wp_1 = -k\delta V(\theta)\left[\frac{2n\Delta}{\beta_\infty}\sin(\alpha + \theta) - \mathrm{Re}\{\exp(-\mathrm{i}\theta)F(\zeta)\}\right]. \tag{4.5}$$

Similar results can be derived for the phase distortions experienced by radiation emitted from the leading edge of blade 1; $\wp_3$ is the phase distortion for a ray which is reflected n times by blade 0 and $n-1$ times by blade 1, while $\wp_4$ is the phase distortion for a ray reflected n times by both blades.

We are now in a position to write down an expression for the field at given point in the blade passage. The unsteady velocity potential takes the form

$$\begin{aligned}
&\sum_{m=0}^{N_-}\int_{-\infty}^{\infty}\frac{g(\theta_0)}{r_0^{1/2}}\exp(\mathrm{i}kwr_0+\mathrm{i}\wp_1)\delta(\xi-\psi-2ms)\,\mathrm{d}\xi\\
&\quad+\sum_{m=1}^{N_+}\int_{-\infty}^{\infty}\frac{g(\theta_0)}{r_0^{1/2}}\exp(\mathrm{i}kwr_0+\mathrm{i}\wp_2)\delta(\xi+\psi-2ms)\,\mathrm{d}\xi\\
&\quad+\sum_{m=1}^{\infty}\int_{-\infty}^{\infty}\frac{g(\theta_1)}{r_1^{1/2}}\exp(\mathrm{i}kwr_1+\mathrm{i}\sigma'+\mathrm{i}\wp_3)\delta(\xi+\psi+(2m-1)s)\,\mathrm{d}\xi\\
&\quad+\sum_{m=0}^{\infty}\int_{-\infty}^{\infty}\frac{g(\theta_1)}{r_1^{1/2}}\exp(\mathrm{i}kwr_1+\mathrm{i}\sigma'+\mathrm{i}\wp_4)\delta(\xi-\psi+(2m+1)s)\,\mathrm{d}\xi,
\end{aligned}\tag{4.6}$$

where the polar coordinates (r_n,θ_n) relative to blade n are now

$$r_n(\xi)=[(\phi-nd)^2+\xi^2]^{1/2},\quad \theta_n(\xi)=\cos^{-1}\left[(\phi-nd)/r_n(\xi)\right],\quad n=0,1,\tag{4.7}$$

with $0<\theta_0<\alpha$ and $3\pi/2<\theta_1<2\pi$. The first two terms in (4.6) correspond to sound which originated at leading edge 0: the first term contains the direct ray plus contributions from the image sources below blade 0, while the second term contains contributions from the image sources above blade 1. The integers $N_\pm$ represent the maximum number of reflections which radiation from leading edge 0 can undergo in its passage to the observer; N_+ corresponds to the radiation which experiences its final reflection en route to the observer from the upper blade, and N_- corresponds to radiation which experiences its final reflection from the lower blade. From simple geometrical arguments it is easy to see that $N_\pm$ are the largest integers smaller than $(\phi\tan\alpha\pm\psi)/2s$ respectively; for an unstaggered cascade, $N_\pm$ are infinite. The third and fourth terms in (4.6) represent sound emanating from leading edge 1: the third term contains contributions from the images lying below blade 0, while the fourth term contains the direct ray plus contributions from the images lying above blade 1. As has already been noted, an infinite number of these image sources contribute to the radiation reaching the observer, since in this case there is no upper limit on the possible number of reflections along the ray path.

The phase distortions along the ray paths are represented by the terms $\wp_i, i=1,2,3,4$, in (4.6), and now take the form

$$\left.\begin{aligned}
\wp_1&=k\delta V(\theta_0)\left[\mathrm{Re}\{\exp(-\mathrm{i}\theta_0)F(\zeta)\}-(\xi-\psi)\left(\frac{\sin(\alpha+\theta_0)}{\beta_\infty\sin\alpha}\right)\right],\\
\wp_2&=k\delta V(\theta_0)\left[\mathrm{Re}\{\exp(\mathrm{i}\theta_0)F(\zeta)\}+(\xi+\psi)\left(\frac{\sin(\alpha-\theta_0)}{\beta_\infty\sin\alpha}\right)\right],\\
\wp_3&=k\delta V(\theta_1)\left[\mathrm{Re}\{\exp(\mathrm{i}\theta_1)F(\zeta)\}+(\xi+\psi-s)\left(\frac{\sin(\alpha-\theta_1)}{\beta_\infty\sin\alpha}\right)\right],\\
\wp_4&=k\delta V(\theta_1)\left[\mathrm{Re}\{\exp(-\mathrm{i}\theta_1)F(\zeta)\}-(\xi-\psi+s)\left(\frac{\sin(\alpha+\theta_1)}{\beta_\infty\sin\alpha}\right)\right].
\end{aligned}\right\}\tag{4.8}$$

In addition to the reflected components, the observer will also receive sound which has been generated at a given leading edge and then diffracted by the other edge. Note, however, that the leading-edge fields already contain the first rescattering of the direct field from a given leading edge, so that any subsequent diffraction is $O(kw)^{-1/2}$ smaller than the reflected fields already described, and is therefore ignored in our analysis.

4.2. *Modal structure*

Equation (4.6) shows that the downstream-propagating field between the blades can be represented by an infinite superposition of cylindrically decaying wave fields, and our aim is now to convert this into the more usual representation as a summation over duct modes. We will only be concerned with calculating the coefficients of the cut-on duct modes, and to do this it will prove convenient to take the limit of large ϕ, so that $N_{\pm} \sim N$ in equation (4.6) with N the integer part of $(\phi \tan\alpha/2s)$. Since the coefficients of the duct modes are necessarily independent of position along the duct, it follows that the values obtained by taking ϕ large are equally valid for $\phi = O(1)$, including at the trailing edge where the cut-on duct modes are scattered into radiation downstream.

We apply Poisson's formula (see Jones 1966 p. 137 and Davies 1985 p. 108) in the form

$$\tfrac{1}{2}(f(N) - f(0)) + \sum_{n=0}^{N-1} f(n) = \sum_{m=-\infty}^{\infty} \int_{-\infty}^{\infty} f(x) \exp(\mathrm{i}2m\pi x)[\mathrm{H}(x) - \mathrm{H}(x-N)]\,\mathrm{d}x \quad (4.9)$$

for an arbitrary function $f(x)$, where $\mathrm{H}(x)$ is the unit step function. We now swap the order of summation and integration in (4.6), apply (4.9), swap the order of summation and integration back and then make the substitution $\xi = \phi\eta$ in the first two integrals and the substitution $\xi = (\phi - d)\eta$ in the second two integrals. Equation (4.6) then becomes

$$\frac{1}{s}\left\{ \frac{1}{\phi^{1/2}} \sum_{m=-\infty}^{\infty} \int_0^{\tan\alpha} \frac{g(\tan^{-1}\eta)}{(1+\eta^2)^{1/4}} \exp(\phi f_1(\eta))\,\mathrm{d}\eta \cos(m\pi\psi/s) \right.$$
$$\left. + \sum_{m=-\infty}^{\infty} \frac{\exp(\mathrm{i}m\pi + \mathrm{i}\sigma')}{(\phi-d)^{1/2}} \int_{-\infty}^{0} \frac{g(\tan^{-1}\eta)}{(1+\eta^2)^{1/4}} \exp((\phi-d) f_2(\eta))\,\mathrm{d}\eta \cos(m\pi\psi/s) \right\}, \quad (4.10)$$

where

$$f_{1,2}(\eta) = \mathrm{i}kw(1+\eta^2)^{1/2} \mp \mathrm{i}m\pi\eta/s. \quad (4.11)$$

The two terms in (4.10) represent sound that emanates from the leading edges of blades 0 and 1, respectively. The arguments of the directivity function $g(\theta)$ represent emission angles; the branches of the inverse tangent functions must be chosen such that $\theta = \tan^{-1}\eta$ lies in the range $0 < \theta_0 < \alpha$ for the first term, and $3\pi/2 < \theta_1 < 2\pi$ for the second term. The factor $\exp(\mathrm{i}m\pi)$ in the second term of (4.10) has arisen from the fact that the leading edge of blade 1 is located on $\psi = s$.

In order to evaluate the integrals in (4.10) asymptotically, we suppose that $k(\phi - d) \gg 1$ and apply the method of stationary phase; it is easy to show that the exponentials in the two integrands in (4.10) possess stationary phase points at

$$\pm\pi m/(k^2w^2s^2 - m^2\pi^2)^{1/2} \quad (4.12)$$

respectively, which lie on the real axis for $|m| < p$, where p is the largest integer smaller than kws/π. Moreover, the stationary point can only lie within the ranges of

integration if $m > 0$. By applying the method of stationary phase to (4.10) we then find, after some considerable algebra, that the modified unsteady velocity potential takes the form

$$\sum_{n=0}^{p} \{ A_u^n + A_l^n \} M^n(\phi, \psi) \exp(-\mathrm{i}k^n \phi), \tag{4.13}$$

where the amplitudes are

$$\left.\begin{aligned} A_l^n &= \frac{\epsilon_n \exp(\mathrm{i}\pi/4)(2\pi k w)^{1/2}}{(k^2 w^2 s^2 - n^2\pi^2)^{1/2}} g(\chi^n) \mathrm{H}(\alpha - \chi^n), \\ A_u^n &= \frac{\epsilon_n \exp(\mathrm{i}\pi/4)(2\pi k w)^{1/2}}{(k^2 w^2 s^2 - n^2\pi^2)^{1/2}} g(2\pi - \chi^n) \exp(\mathrm{i}\sigma' + \mathrm{i}n\pi + \mathrm{i}k^n d + \mathrm{i}\kappa^n), \end{aligned}\right\} \tag{4.14}$$

the axial duct wavenumbers are

$$k^n = -(k^2 w^2 - (n\pi/s)^2)^{1/2}, \tag{4.15}$$

with associated mode angle $\chi^n = \cos^{-1}(-k^n/kw)$, the modal functions $M^n(\phi, \psi)$ are

$$M^n(\phi, \psi) = \cos\left[\frac{n\pi\psi}{s} + \Theta^n(\phi, \psi)\right] \exp(\mathrm{i}\Xi^n(\phi, \psi)), \tag{4.16}$$

and the phase distortions are

$$\left.\begin{aligned} \Theta^n(\phi, \psi) &= \frac{k\delta V(\chi^n) \sin\chi^n}{\beta_\infty} \left[\frac{\psi}{\tan\alpha} - \phi\right] + k\delta V(\chi^n) \sin\chi^n \mathrm{Im}[F(\zeta)], \\ \Xi^n(\phi, \psi) &= \frac{k\delta V(\chi^n)}{\beta_\infty \cos\chi^n} \left[\psi \cos^2\chi^n - \frac{\phi \sin^2\chi^n}{\tan\alpha}\right] + k\delta V(\chi^n) \cos\chi^n \mathrm{Re}[F(\zeta)], \\ \kappa^n &= \frac{k\delta V(\chi^n)\Delta}{\beta_\infty \sin\alpha \cos\chi^n} [\cos^2\alpha - \cos^2\chi^n]. \end{aligned}\right\} \tag{4.17}$$

It is well known that the field between the blades is in fact composed of an infinite superposition of duct modes with ϕ wavenumbers k^n, $n = 0, 1, \ldots$, but for $n > p$ we see that k^n is imaginary, and the duct mode is cut off and does not propagate downstream from the leading-edge region. We have presented only expressions for the cut-on mode amplitudes, since it is only the cut-on duct modes which will interact with the cascade trailing edges, and which will therefore be required when we come to predict the radiation downstream of the cascade.

4.3. *Discussion of modal results*

We note that $\Theta^n(\phi, \psi)$, $\Xi^n(\phi, \psi)$ and κ^n in (4.17) are $O(k\delta)$, and are therefore significant, and that in deriving (4.17) we have neglected terms of $O(\delta)$. It is easy to show that, when $\delta = 0$, the modal function $M^n(\phi, \psi)$ reduces to the uniform-flow duct mode $\cos(n\pi\psi_0/s_0)$. It is not at first sight clear that the new modal functions $M^n(\phi, \psi)$ have zero normal velocity on the blades, i.e. that $\partial M^n/\partial\psi = 0$ to the asymptotic order considered on $\psi = 0$, $\psi = s$. However, using the expression (2.7) for the value of $\mathrm{Im}[F]$ on the blade surfaces, it can be shown that $\Theta^n(\phi, \psi) = 0$ and $\partial\Xi(\phi, \psi)/\partial\psi = 0$ on $\psi = 0$, $\psi = s$, from which the required normal-velocity condition follows immediately.

In order to interpret the corresponding phase distortions we first note that the terms involving $\mathrm{Re}[F(\zeta)]$ and $\mathrm{Im}[F(\zeta)]$ in (4.17) have arisen from the distortion of the waves as they propagate between their last reflection by the blades and the observer (this is clear from the derivation of the expressions for $\wp_2$ etc.), while the

other terms in (4.17) arise from the previous multiple reflections between the blades. We consider first the plane-wave case $n=0$, in which to leading order the wave propagation direction is aligned parallel to the ϕ-axis (since $\chi^0=0$), and in physical space therefore parallel to the steady-flow streamlines. Clearly $\Theta^0(\phi,\psi)=0$, and we can therefore say immediately that $\Theta^n(\phi,\psi)$ corresponds to the distortion of the cross-stream wavenumber which arises as a result of the propagation of the wave in the cross-stream direction, and this interpretation is of course confirmed by the fact that $\Theta^n(\phi,\psi)\propto\sin\chi^n$. In contrast, we note that only the second term in $\Xi^n(\phi,\psi)$ vanishes for $n=0$, and it follows that the first term in $\Xi^n(\phi,\psi)$ is the distortion of the cross-stream wavenumber arising from streamwise propagation, while the second term is the distortion which arises from cross-stream propagation (and is therefore absent for $n=0$).

The amplitude factor A_u^n for the radiation from the upper leading edge contains several additional phase factors. The term σ' arises from the global periodicity property of the solution, the term $n\pi$ arises from the basic symmetry property of the mode of order n, and the term $k^n d$ accounts for the streamwise displacement of the upper leading edge relative to the lower. These three phase terms are $O(k)$ and are present for the case $\delta=0$ as well. The last term in the phase, κ^n, is $O(k\delta)$ and is an additional phase distortion for the waves emitted from the upper leading edge, related to the fact that the steady flow is asymmetric about the duct centreline when $\delta\neq 0$.

We note that (4.13) possesses a jump discontinuity when $\chi^n=\alpha$, which corresponds to the coincidence between the propagation angle and the front face of the cascade. The expression is also non-uniform at duct mode cut-off, because the stationary-phase point (4.12) then approaches infinity. This effect occurs for both non-zero mean loading and uniform flow, but the cut-off condition differs in each case. For $\delta\neq 0$ the cut-off condition is $n=kws/\pi$, compared to the zero-mean-loading condition $n=kws_0/\pi$. It is easy to show that $s=\Delta_*\beta_\infty\sin(\alpha_*-\delta)/b_*$, so that for acute α_* we have $s<s_0$. It therefore follows that one effect of non-zero mean loading is to potentially change the number of modes which are cut on between the blades; if $\alpha_*<\pi/2$ is kept fixed then increasing the mean loading will reduce the number of cut-on modes.

It is interesting to consider the evolution of the duct modes far downstream. If we were to suppose that the blades continue indefinitely in the downstream direction (which is of course not the case in practice), then the steady flow would approach a uniform stream aligned parallel to the blades. The speed of this steady flow can be found conveniently by applying mass conservation to the incompressible flow in the Prandtl–Glauert plane, in which the cascade has stagger angle α and inclination $\delta\beta_\infty^{-1}$ to the upstream flow. Far downstream, we then find the values

$$\delta q=-\frac{\delta}{\beta_\infty\tan\alpha},\qquad \delta\mu=-\frac{\delta}{\beta_\infty},\qquad \delta F(\zeta)=\left[\frac{\mathrm{i}\delta}{\beta_\infty}-\frac{\delta}{\beta_\infty\tan\alpha}\right]\zeta+\text{const.} \tag{4.18}$$

From (4.17) it follows that downstream $\Theta^n(\phi,\psi)\to 0$, and that the duct modes take the form

$$\cos\left[\frac{n\pi\psi}{s}\right]\exp\left[\mathrm{i}\left(kw\cos\chi^n-\frac{\mathrm{i}k\delta V(\chi^n)}{\beta_\infty\tan\alpha\cos\chi^n}\right)\phi\right]. \tag{4.19}$$

These are precisely the modes for a duct containing the uniform downstream flow; this can be verified by standard duct acoustic formulae, or by the dispersion relation

formed from the homogeneous version of (2.11), using (2.13) with δq, $\delta\mu$ given by (4.18).

Finally, we consider modes which are close to cut-off, in which case n is close to kws/π and χ^n is close to $\pi/2$. Such modes propagate almost perpendicular to the stream, and therefore experience a considerable number of multiple reflections and cross-stream phase distortion before reaching the observer. Indeed, we can see that the phase distortion $\Xi^n(\phi, \psi)$ becomes large, and in fact diverges as

$$-\frac{k\delta V(\pi/2)\phi}{\beta_\infty \tan\alpha \cos\chi^n}, \tag{4.20}$$

and will become significant compared to the leading-order ϕ phase term $\phi kw \cos\chi^n$. (We note that, since Θ^n remains bounded as $\chi^n \to \pi/2$, the distortion to the ψ phase term remains uniformly smaller than the leading-order term $n\pi\psi/s$.) For the two-dimensional case $k_z = 0$, the sign of $V(\pi/2)$ is negative for $M_\infty < 0.59$ while it is positive for $M_\infty > 0.59$. Thus, for $M_\infty < 0.59$ the phase distortion (4.20) acts to increase the ϕ wavenumber, while for $M_\infty > 0.59$ this term acts to decrease the ϕ wavenumber. In the latter case the phase distortion involved in the repeated reflections has the effect of tilting the phase vector of a nearly cut-off mode closer to the cross-stream direction. By looking at the expression (4.19) for the modal structure far downstream, it is therefore clear that a mode which is already close to cut-off near the leading edges will be propagating even closer to the cross-stream direction as it propagates further downstream. This is an important fact, because it suggests that modes which are cut on near the start of the blade passage can become cut off further down the blade passage, and must therefore turn round and propagate back upstream. Of course, the stationary-phase analysis used to determine the modal structure is non-uniform at $\chi^n = \pi/2$, since then the stationary-phase point approaches infinity (see (4.12)), and further work needs to be done to derive a uniform asymptotic approximation for this process.

We will see in §6 that the number of radiation modes cut on downstream of the cascade can differ from the number cut on upstream of the cascade. This difference arises from the change in inclination of the steady flow to the front face of the cascade which is induced by the mean loading. It is not related directly to the issue of duct modes turning round somewhere along the blade passage. This can be seen by noting that the radiation-mode wavenumbers (6.28) are determined by the periodicity property (2.9) of the cascade, while the duct-modes wavenumbers (4.15) are determined by the boundary condition (2.15) on the blade surfaces.

5. Downstream formulation

In the next section we will calculate the sound field downstream of the cascade, but before we do this it will be necessary to make a transformation from the present ϕ–ψ coordinates based on the upstream steady flow to new potential–streamfunction coordinates based on the downstream steady flow. The need for this transformation can be seen by noting that, although the steady flow through the cascade approaches its upstream and downstream limits exponentially rapidly, these two limits are different. Therefore, while the perturbation potential $F(\zeta)$ approaches a constant value far upstream, it grows linearly in ζ far downstream, leading to a secular term which obscures the modal structure of the downstream radiation. Indeed, we believe that one of the key features of any cascade noise prediction method is that the cut-off frequencies of the radiation modes are predicted correctly. The coordinates of

§2 lead to exact expressions for the modal cut-off frequencies upstream (see (I)), but the presence of the secular term mentioned above means that we need to introduce new coordinates to obtain the exact cut-off frequencies downstream. Moreover, ϕ is discontinuous across the blade wakes in physical space, and for convenience it is sensible to introduce coordinates which vary continuously downstream. It should be noted that the cascade not only turns the oncoming flow, but also changes the steady-flow Mach number and density, and this means that as well as changing coordinates it will also prove convenient to use the downstream, instead of the upstream, steady-flow speed and density to non-dimensionalize physical variables.

5.1. *Downstream steady flow*

We denote the downstream steady speed and density and the inclination of the blades to the downstream flow by $\bar{U}_\infty$, $\bar{\rho}_\infty$ and $\bar{\delta}$ respectively, and in what follows an overbar will be used to denote downstream variables. First, we introduce physical coordinates $(\bar{x}_*, \bar{y}_*)$ aligned with the downstream steady flow, which are obtained by rotating the upstream axes (x_*, y_*) through an angle $\delta - \bar{\delta}$ in the clockwise sense (see figure 1), but with origin at the trailing edge of blade 0. We then transform to potential–streamfunction coordinates based on the downstream flow,

$$\left.\begin{aligned} \bar{\psi} &= \frac{\bar{\beta}_\infty U_\infty}{\beta_\infty \bar{U}_\infty}\psi, \\ \bar{\phi} &= \frac{U_\infty}{\bar{U}_\infty}(\phi - l^+ + m\Gamma) \quad \text{when} \quad m\bar{s} \leqslant \psi < (m+1)\bar{s}. \end{aligned}\right\} \tag{5.1}$$

These new coordinates have been chosen so that the trailing edges of the upper and lower surfaces of a given blade map onto the same point in $\bar{\phi}$–$\bar{\psi}$ space, with the origin at the trailing edge of blade 0. Mathematically, these new coordinates have the effect of transferring the branch cut associated with the blade circulation from downstream of the trailing edges to upstream (each leading edge now maps onto two points in $\bar{\phi}$–$\bar{\psi}$ space), and are therefore exactly analogous to the trailing-edge coordinates adopted for the single airfoil by Myers & Kerschen (1995). The physical cascade then maps onto a cascade in $\bar{\phi}$–$\bar{\psi}$ space (see figure 4), with stagger angle $\bar{\alpha}$ and trailing-edge separation $\bar{\Delta}$, where $\bar{\alpha}$ and $\bar{\Delta}$ are obtained from (2.2) and (2.3) by replacing δ and β_∞ by $\bar{\delta}$ and $\bar{\beta}_\infty$, respectively. The trailing edge of blade m is mapped to $(\bar{\phi}, \bar{\psi}) = (m\bar{d}, m\bar{s})$, where $\bar{d} = \bar{\Delta}\cos\bar{\alpha}$, $\bar{s} = \bar{\Delta}\sin\bar{\alpha}$.

As in §2, the steady flow through the cascade can be determined by thin-airfoil theory and conformal mapping. Here, however, we utilize a Prandtl–Glauert transformation based on the downstream flow, and it follows that the velocity potential and streamfunction have the expansion

$$\bar{\zeta} = \bar{\zeta}_0 + \bar{\delta}\bar{F}(\bar{\zeta}_0), \tag{5.2}$$

where $\bar{\zeta} = \bar{\phi} + \mathrm{i}\bar{\psi}$, $\bar{\zeta}_0 = \bar{\phi}_0 + \mathrm{i}\bar{\psi}_0 = (\bar{x}_* + \mathrm{i}\bar{\beta}_\infty \bar{y}_*)/b_*$ and the arbitrary constant in $\bar{F}(\bar{\zeta})$ is chosen such that $\bar{F}(0) = 0$. Since $\bar{\zeta} = \bar{\zeta}_0 + O(\bar{\delta})$, the mean flow perturbation is given by

$$\bar{q} - \mathrm{i}\bar{\mu} = \frac{\mathrm{d}\bar{F}(\bar{\zeta})}{\mathrm{d}\bar{\zeta}}, \tag{5.3}$$

where the normalized flow speed is $U_*/\bar{U}_\infty = 1 + \bar{\delta}\bar{q}$ and the flow angle is $\bar{\delta}\bar{\beta}_\infty\bar{\mu}$. From the inclination of the blades to the downstream flow, it is clear that $\bar{\mu} = -1/\bar{\beta}_\infty$ on the blade surfaces, and the imaginary part of (5.3) can then be integrated to give the

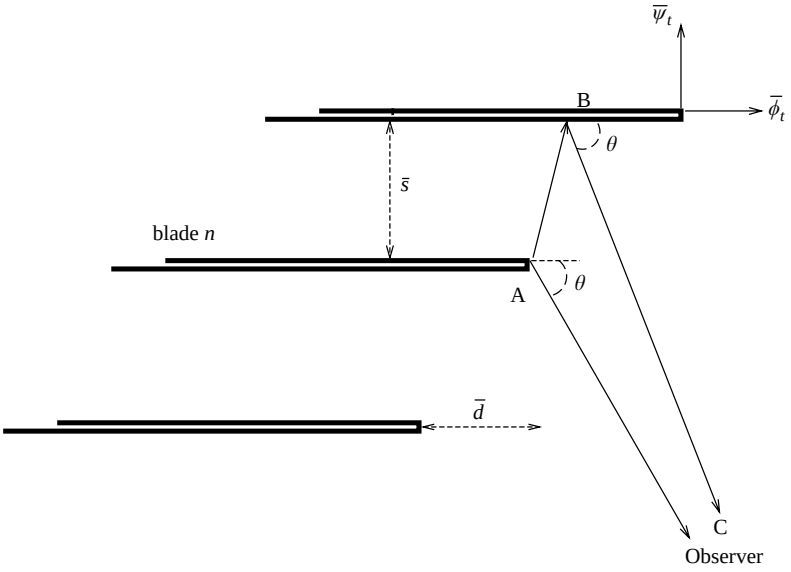

FIGURE 4. The cascade geometry in $\bar{\phi}$–$\bar{\psi}$ space. The ray paths of the downstream direct and reflected rays are illustrated.

value of $\mathrm{Im}[\bar{F}]$ on blade m in the form

$$\mathrm{Im}[\bar{F}] = \frac{(\bar{\phi} - m\bar{d})}{\bar{\beta}_\infty}. \tag{5.4}$$

This result will be utilized in calculating the phase distortions in the downstream field.

The upstream and downstream steady flow fields are related by the conservation relations

$$\left.\begin{aligned} &\bar{\rho}_\infty \bar{U}_\infty \sin(\alpha_* - \bar{\delta}) = \rho_\infty U_\infty \sin(\alpha_* - \delta), \\ &-\Gamma U_\infty b_* = \Delta_* [U_\infty \cos(\alpha_* - \delta) - \bar{U}_\infty \cos(\alpha_* - \bar{\delta})]. \end{aligned}\right\} \tag{5.5}$$

These results are exact and follow by considering a channel formed by adjacent stagnation streamlines and the corresponding blades; the first equation comes from mass conservation, while the second is obtained by integrating round this contour in the clockwise direction and using the definition of blade circulation. The circulation is determined from the conformal mapping by applying the Kutta condition at the trailing edge. Then, linearizing (5.5) about the upstream flow and using general relations for small-perturbation isentropic flow, the flow deflection across the cascade is

$$\bar{\delta} - \delta = \Gamma \beta_\infty \sin\alpha / \Delta. \tag{5.6}$$

The upstream flow area associated with a single blade passage is $\Delta_* \sin(\alpha_* - \delta)$, while the downstream flow area is $\Delta_* \sin(\alpha_* - \bar{\delta})$. The downstream mean flow quantities $\bar{U}_\infty$, $\bar{\rho}_\infty$ and $\bar{M}_\infty$ are then given, in terms of the corresponding upstream quantities and the passage area ratio, by the relations for one-dimensional isentropic flow.

The mean flow perturbation due to the cascade dies off exponentially with distance downstream (based on the lengthscale $\bar{\Delta}$), so that $\bar{F}(\bar{\zeta})$ reaches its downstream asymptotic limit $\bar{F}(\infty)$ quite rapidly. The quantity $\bar{F}(\infty)$ depends on the cascade parameters, and can be determined from the conformal mapping. In fact, $\bar{\delta}\bar{F}(\infty)$ is

a measure of the phase distortion experienced by the downstream radiation – cf. equation (5.20) of (I). In practice, the cascade acts to turn the incoming flow, so that $\bar{\delta}$ is always smaller (and perhaps even much smaller) than δ. Thus, the phase distortion introduced in propagation from the cascade to the downstream region is much less than that introduced in propagation from the cascade to the upstream region.

5.2. *Downstream unsteady flow*

In parallel with (2.10) and (2.17), the total unsteady velocity potential and the unsteady pressure are now written in terms of the new, downstream modified potential $\bar{h}(\bar{\phi}, \bar{\psi})$ in the form

$$\epsilon \bar{U}_\infty b_* \bar{h}(\bar{\phi}, \bar{\psi}) \exp([\mathrm{i}\bar{k}[\bar{k}_z z - \bar{t} - \bar{M}_\infty^2 \bar{\phi}/\bar{\beta}_\infty^2]) \exp(\bar{\delta} \bar{M}_\infty^2 \bar{q}) \tag{5.7}$$

and

$$\epsilon \bar{\rho}_\infty \bar{U}_\infty^2 \left[\mathrm{i}\frac{\bar{k}}{\bar{\beta}_\infty^2} \bar{h} - \frac{\partial \bar{h}}{\partial \bar{\phi}} \right] \exp(\mathrm{i}\bar{k}[\bar{k}_z z - \bar{t} - \bar{M}_\infty^2 \bar{\phi}/\bar{\beta}_\infty^2]) \tag{5.8}$$

respectively. Here $\bar{t} = \bar{U}_\infty t_*/b_*$ and $\bar{k} = \omega_* b_*/\bar{U}_\infty$ are the new non-dimensional time and gust reduced frequency, respectively. The relation between the downstream and upstream reduced frequencies is simply $\bar{k} = kU_\infty/\bar{U}_\infty$. Note also that the spanwise wavenumber is unaffected by the coordinate transformation, so that $\bar{k}\bar{k}_z = kk_z$.

It is then necessary to re-express the duct-mode field (4.13) in terms of trailing-edge coordinates. The duct-mode propagation angle and streamwise wavenumber change by $O(\delta)$ amounts in transforming between the upstream and downstream Prandtl–Glauert spaces. For the duct mode of order n, the propagation angle $\bar{\chi}^n$ satisfies $\bar{k}\bar{w} \sin \bar{\chi}^n = n\pi/\bar{s}$, and the corresponding streamwise wavenumber is $\bar{k}^n = -\bar{k}\bar{w} \cos \bar{\chi}^n$, where $\bar{w}$ is obtained by replacing the upstream variables by the corresponding downstream variables in (2.12). After some algebra it turns out that the unsteady velocity potential of a single duct mode from (4.13), in the passage between blade 0 and blade 1, takes the form

$$\bar{A}^n \cos\left[\frac{n\pi\bar{\psi}}{\bar{s}} + \bar{\Theta}^n \right] \exp(-\mathrm{i}\bar{k}^n \bar{\phi} + \mathrm{i}\bar{k}\bar{\delta}\bar{\mathscr{F}}^n), \tag{5.9}$$

where

$$\bar{k}\bar{\delta}\bar{\mathscr{F}}^n(\bar{\phi}, \bar{\psi}) = \bar{\Xi}^n(\bar{\phi}, \bar{\psi}) + \bar{\phi}\left(\frac{\bar{k}\bar{M}_\infty^2}{\bar{\beta}_\infty^2} - \frac{\bar{U}_\infty k M_\infty^2}{U_\infty \beta_\infty^2} - \bar{k}\bar{w} \cos \bar{\chi}^n + \frac{\bar{U}_\infty}{U_\infty} k w \cos \chi^n \right), \tag{5.10}$$

and where the complex amplitude is given by

$$\bar{A}^n = \left(A_u^n + A_l^u \right) \exp(-\mathrm{i}l^+[k^n + kM_\infty^2/\beta_\infty^2]). \tag{5.11}$$

In deriving (5.9) we have neglected small terms of size $O(\delta)$ in the expansion of the amplitude $\bar{A}^n$ (so for instance a factor $\rho_\infty U_\infty^2/\bar{\rho}_\infty \bar{U}_\infty^2$, arising from the change in the pressure normalization between upstream and downstream coordinates, has been set equal to unity). We have $\bar{\Theta}^n(\bar{\phi}, \bar{\psi}) \equiv \Theta^n(\phi, \psi)$ and $\bar{\Xi}^n(\bar{\phi}, \bar{\psi}) \equiv \Xi^n(\phi, \psi)$, corresponding to the cross-stream and streamwise phase distortions induced by propagation though the non-uniform flow. The total streamwise phase distortion term $\bar{k}\bar{\delta}\bar{\mathscr{F}}^n(\bar{\phi}, \bar{\psi})$ also contains additional terms corresponding to the change in the effective duct mode angle, Mach number and reduced frequency when transforming from upstream Prandtl–Glauert space to downstream Prandtl–Glauert space. The phase factor in the amplitude (5.11) comes from replacing ϕ by $\bar{\phi}$ in (4.13).

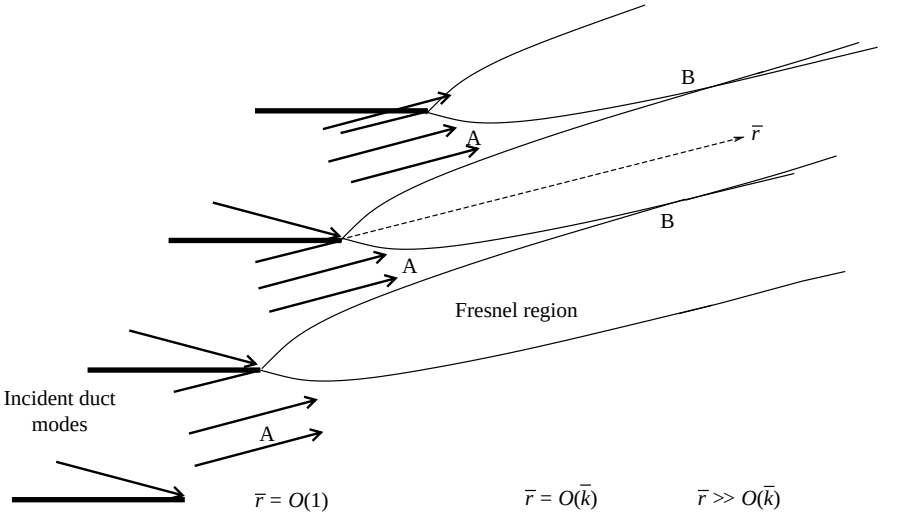

FIGURE 5. Schematic diagram of downstream radiation for a single duct mode, and the Fresnel regions emanating from each edge, for the case $\bar{\chi}^n < \bar{\alpha}$. (For clarity, only the regions associated with the upward-propagating component of the duct mode are shown; the corresponding regions for the downward-propagating component have been omitted.) In region A the radiation is dominated by direct radiation from the passages. The Rayleigh distance, where the Fresnel regions from adjacent edges overlap, is denoted B, while far downstream of B the field is dominated by the diffracted fields from each edge.

6. Downstream radiation

We now move on to consider the downstream radiation. There are significant differences in the nature of the downstream radiation, relative to the upstream radiation analysed in (I). For the upstream radiation, the sound is effectively produced by point sources at the leading edge of each blade; the primary issue is then the conversion of this infinite set of cylindrical wave fields into the propagating plane-wave modes for the uniform flow upstream of the cascade. In contrast, the sound source for the downstream radiation is the duct modes propagating down the blade passages, and their scattering by the trailing edges. The field in the near downstream region is dominated by direct radiation of duct-mode 'beams' from the rear of the blade passages. However, Fresnel regions appear along the edges of these beams, associated with the diffraction of the incident duct modes by the trailing edges. The width of these Fresnel regions grows with distance downstream, and they eventually spread to completely encompass the duct-mode beams, at a distance $O(k)$. Further downstream the beams essentially disappear, and the radiation is dominated by the diffraction fields from each trailing edge. This process is shown schematically in figure 5, and the detailed analysis will be presented as follows:

§6.1 The near-downstream region, dominated by direct radiation from the passages, marked A in figure 5.

§6.2 The diffracted field produced by scattering at the lower trailing edge of each passage.

§6.3 The diffracted field produced by scattering at the upper trailing edge of each passage.

§6.4 The far-downstream field produced by the merging of the fields from adjacent trailing edges.

§6.5 The total cascade radiation, produced by summing contributions from each passage, in both region A and far downstream of region B in figure 5.

6.1. *Radiation from a single blade passage for* $\bar{r} = O(1)$

First consider the field radiated from the blade passage between blades 0 and 1, for downstream distances $\bar{r} = O(1)$. In this region, marked 'A' in figure 5, the downstream field is a simple extension of the duct-mode field that exists within the blade passage. The expression for a single duct mode of order n is given by (5.9). Writing the cosine in terms of exponentials, it can be seen that the duct mode is a superposition of two nearly planar waves propagating at angles $\pm\bar{\chi}^n$ with respect to the $\bar{\phi}$-axis, which are repeatedly reflected and re-reflected by the blades. The downstream radiation pattern is different, depending on whether the duct-mode propagation angle $\bar{\chi}^n$ is less than or greater than the cascade stagger angle $\bar{\alpha}$, and these two cases will be discussed separately.

For the case $\bar{\chi}^n < \bar{\alpha}$, the field at $O(1)$ distances downstream of the cascade consists of two beams, extending into the downstream region at angles $\pm\bar{\chi}^n$. The modified potential for this field has the form

$$\frac{\bar{A}^n}{2}\Bigg[\{H(\bar{\phi}+\bar{\psi}\cot\bar{\chi}^n)-H(\bar{\phi}-\bar{d}+(\bar{\psi}-\bar{s})\cot\bar{\chi}^n)\}\exp(\mathrm{i}\bar{k}\bar{w}[\bar{\phi}\sin\bar{\chi}^n-\bar{\psi}\cos\bar{\chi}^n]$$
$$+\mathrm{i}\bar{k}\bar{\delta}[\bar{\mathscr{F}}^n(\bar{\phi},\bar{\psi})-\bar{\Theta}^n(\bar{\phi},\bar{\psi})])\Bigg]+\frac{\bar{A}^n}{2}\Bigg[\{H(\bar{\phi}-\bar{d}-(\bar{\psi}-\bar{s})\cot\bar{\chi}^n)-H(\bar{\phi}-\bar{\psi}\cot\bar{\chi}^n)\}$$
$$\times\exp(\mathrm{i}\bar{k}\bar{w}[\bar{\phi}\sin\bar{\chi}^n+\bar{\psi}\cos\bar{\chi}^n]+\mathrm{i}\bar{k}\bar{\delta}[\bar{\mathscr{F}}^n(\bar{\phi},\bar{\psi})+\bar{\Theta}^n(\bar{\phi},\bar{\psi})])\Bigg], \tag{6.1}$$

where the first set of terms in large square brackets corresponds to a downward-propagating beam of width $\bar{\Delta}\sin(\bar{\alpha}+\bar{\chi}^n)$, while the second set of terms in large square brackets corresponds to an upward-propagating beam of width $\bar{\Delta}\sin(\bar{\alpha}-\bar{\chi}^n)$. For a staggered cascade, the upward-propagating beam is narrower than the downward-propagating beam. Note that the width of the upper beam approaches zero as $\bar{\chi}^n \to \bar{\alpha}$. Within the two beams, the phase distortion due to the mean flow variations is given by $\bar{k}\bar{\delta}[\bar{\mathscr{F}}^n(\bar{\phi},\bar{\psi}) \mp \bar{\Theta}^n(\bar{\phi},\bar{\psi})]$. The mean flow perturbation $\mathrm{d}\bar{F}/\mathrm{d}\bar{\zeta}$ decays to zero exponentially with distance downstream, so that the phase distortion functions approach their asymptotic downstream values within about one passage width downstream of the cascade. The asymptotic values for $\bar{\mathscr{F}}^n$ and $\bar{\Theta}^n$ are obtained by replacing $\bar{F}(\bar{\zeta})$ with $\bar{F}(\infty)$.

For $\bar{\chi}^n > \bar{\alpha}$, the upward beam is completely blocked by the lower surface of blade 1. In this case the downstream edge of the downward-propagating beam is determined not by the location of the trailing edge of blade 1, but rather by the location where the wave that is reflected from the trailing edge of blade 0 is re-reflected by blade 1. The width of the downward-propagating beam in this case is $2\bar{s}\cos\bar{\chi}^n$, and the modified potential takes the form

$$\frac{\bar{A}^n}{2}\{H(\bar{\phi}+\bar{\psi}\cot\bar{\chi}^n)-H(\bar{\phi}+(\bar{\psi}-2\bar{s})\cot\bar{\chi}^n)\}\exp(\mathrm{i}\bar{k}\bar{w}[\bar{\phi}\sin\bar{\chi}^n-\bar{\psi}\cos\bar{\chi}^n]$$
$$+\mathrm{i}\bar{k}\bar{\delta}[\bar{\mathscr{F}}^n(\bar{\phi},\bar{\psi})-\bar{\Theta}^n(\bar{\phi},\bar{\psi})]). \tag{6.2}$$

The comments following (6.1) concerning the $O(\bar{k}\bar{\delta})$ phase distortion terms are applicable here as well.

In addition to the beams contained in (6.1) and (6.2), the downstream field for a single passage also contains cylindrically spreading waves associated with diffraction of the duct mode by the trailing edge of blade 0, and also by the trailing edge of blade 1 for the case $\bar{\chi}^n < \bar{\alpha}$. These diffracted fields are calculated in the following

subsection. We will also show that the diffraction process generates Fresnel regions along the edges of the beams, which serve to smooth the discontinuities present in (6.1) and (6.2).

6.2. *Scattering by the lower trailing edge*

The component of the duct mode propagating at angle $-\bar{\chi}^n$ impinges on the trailing edge of the lower blade for all values of $\bar{\chi}^n$, and this scattering process will be considered first. For $\bar{\chi}^n < \bar{\alpha}$, the component of the duct mode propagating at angle $\bar{\chi}^n$ impinges on the trailing edge of the upper blade, and this scattering process will be considered in the next subsection. For $\bar{\chi}^n > \bar{\alpha}$, the component of the duct mode propagating at angle $\bar{\chi}^n$ does not reach the trailing edge of the upper blade, so that the duct mode is scattered only by the trailing edge of the lower blade of the passage.

First consider the scattering of the duct mode by the trailing edge of the lower blade. For definiteness, we consider the passage lying between blades 0 and 1. To analyse the diffraction field generated by this interaction, we consider an inner region of size $O(1/k)$ around the trailing edge, and introduce the inner coordinates $\bar{\Phi} = \bar{k}\bar{\phi}$, $\bar{\Psi} = \bar{k}\bar{\psi}$. The inner expansion of the duct mode (5.9) consists of an incident plane wave propagating at angle $-\bar{\chi}^n$ and a reflected plane wave propagating at angle $\bar{\chi}^n$. The total field in the inner region then consists of the incident and reflected plane waves in $\bar{\Psi} > 0$, supplemented by a scattered field $\bar{H}(\bar{\Phi}, \bar{\Psi})$.

Expanding (2.11) in the inner region, following Myers & Kerschen (1995), it can be shown that the modified potential $\bar{H}(\bar{\phi}, \bar{\psi})$ satisfies the homogeneous Helmholtz equation

$$\frac{\partial^2 \bar{H}}{\partial \bar{\Phi}^2} + \frac{\partial^2 \bar{H}}{\partial \bar{\Psi}^2} + \bar{w}^2 \bar{H} = 0, \tag{6.3}$$

where $\bar{w}$ is obtained by replacing the upstream variables by the corresponding downstream variables in (2.12). In contrast to the leading-edge flow, we see that to the asymptotic order considered there are no volume sources in the vicinity of the trailing edge, essentially due to the fact that the local steady flow satisfies the Kutta condition, and therefore possesses much weaker gradients than are present at the leading edge. (We also note that no radiation is generated when the convected gusts pass the trailing edge, since the gusts are convected with the local free-stream speed and induce no pressure fluctuations. Further discussion can be found in Myers & Kerschen 1995.)

The combination of incident and reflected plane waves satisfies the boundary condition (2.15) on the upper surface of blade 0. Therefore, the scattered field satisfies the homogeneous boundary conditions

$$\frac{\partial \bar{H}}{\partial \bar{\Psi}}(\bar{\Phi}, \pm 0) = 0 \quad \text{for} \quad \bar{\Phi} < 0 \tag{6.4}$$

on the upper and lower surfaces of blade 0.

The combination of incident and reflected waves produces a non-zero pressure field on $\bar{\Psi} = +0$,

$$\overline{\Delta p}_n \exp(\mathrm{i}[\bar{w} \cos \bar{\chi}^n - \bar{M}_\infty^2 / \bar{\beta}_\infty^2]\bar{\Phi}), \tag{6.5}$$

where

$$\overline{\Delta p}_n = \mathrm{i} \left(\bar{k}^n + \frac{\bar{k}}{\bar{\beta}_\infty^2} \right) \bar{A}^n \exp(-\mathrm{i}\bar{k}^n l^+ + \mathrm{i}\bar{k}\bar{\delta}\mathscr{F}^n(0,0)). \tag{6.6}$$

Equation (6.5) has been derived by noting that, when determining the unsteady pressure from the modified velocity potential, the $\bar{\phi}$ derivatives of $\bar{\Xi}^n(\bar{\phi}, \bar{\psi})$ and

$\bar{\Theta}^n(\bar{\phi}, \bar{\psi})$ can be neglected in our high-frequency limit. Also, we have used the fact that close to the trailing edge, and to the asymptotic order considered, we can make the replacement $\bar{\Xi}^n(\bar{\phi}, 0) \to \bar{\Xi}^n(0, 0)$. The scattered field must cancel this pressure jump, leading to the boundary condition

$$\left(\mathrm{i}\frac{\bar{k}}{\bar{\beta}_\infty^2}\bar{H} - \bar{k}\frac{\partial \bar{H}}{\partial \bar{\Phi}}\right)\Bigg|_{\bar{\Psi}=-0}^{\bar{\Psi}=+0} = -\overline{\Delta p}_n \exp(\mathrm{i}\bar{w}\cos\bar{\chi}^n\bar{\Phi}) \quad \text{for} \quad \bar{\Phi} > 0. \tag{6.7}$$

In general, vorticity can be shed from the trailing edge and therefore $\bar{H}(\bar{\Phi}, \bar{\Psi})$ and $\partial\bar{H}/\partial\bar{\Phi}$ are discontinuous across $\bar{\Psi} = 0$ for $\bar{\Phi} > 0$. However, the normal velocity is continuous across the trailing vortex sheet, so that

$$\frac{\partial \bar{H}}{\partial \bar{\Psi}}\Bigg|_{\bar{\Psi}=-0}^{\bar{\Psi}=+0} = 0 \quad \text{for} \quad \bar{\Phi} > 0. \tag{6.8}$$

Finally, the unsteady Kutta condition applies at the trailing edge, so that the first-order derivatives of $\bar{H}(\bar{\Phi}, \bar{\Psi})$ must be finite in the vicinity of $\bar{\Phi} = \bar{\Psi} = 0$.

The same boundary-value problem is solved in Myers & Kerschen (1995); additional phase factors are present in their formulation (see equations (3.47, 48) of that paper). These phase factors arise in their work from the exponential term $\exp(-\mathrm{i}kM_\infty^2\phi/\beta_\infty^2)$ in the relationship between the total unsteady velocity potential and h (see our (2.10)), but are absent here since the corresponding phase factor in our definition (5.7) involves the variable $\bar{\phi}$ based on the downstream flow. Of course, the solutions for physical quantities, such as the total unsteady potential and the pressure, are exactly equivalent.

The scattered potential $\bar{H}(\bar{\Phi}, \bar{\Psi})$ can be determined using Fourier transform methods and the Wiener–Hopf technique. The solution is

$$\bar{H}(\bar{\Phi}, \bar{\Psi}) = \frac{\mathrm{i}(2\bar{w})^{1/2}}{4\pi\bar{k}}\mathrm{sgn}(\bar{\Psi})\overline{\Delta p}_n \cos\tfrac{1}{2}\bar{\chi}^n \int_{-\infty}^{\infty} \frac{\exp\left(-\mathrm{i}\bar{\Phi}\lambda - |\bar{\Psi}|(\lambda^2 - \bar{w}^2)^{1/2}\right)}{(\lambda - \bar{w})^{1/2}(\lambda + \bar{\beta}_\infty^{-2})(\lambda + \bar{w}\cos\bar{\chi}^n)}\,\mathrm{d}\lambda, \tag{6.9}$$

where the square roots in the integrand are defined by introducing branch cuts parallel to the imaginary axis and joining $\pm\bar{w}$ to infinity through the upper and lower half-planes, with the values of the square roots at the origin being taken as negative imaginary. The inversion contour passes above the poles at $\lambda = -\bar{\beta}_\infty^{-2}$ and $-\bar{w}\cos\bar{\chi}^n$. Therefore, these poles contribute for $\bar{\Phi} > 0$. The residue of the first pole produces the vortex sheet that is shed from the trailing edge. For $\bar{\Psi} < 0$, the residue of the second pole produces the downward-propagating plane wave of (6.1) and (6.2), while for $\bar{\Psi} < 0$ it cancels the upward-propagating reflected plane wave component of the original duct mode.

The method of steepest descents is now used to evaluate the outer limit of the inner potential (6.9), which is then matched onto an outgoing cylindrically decaying ray field in the outer region in exactly the same way as described in Myers & Kerschen (1995). We find that the outer unsteady potential from blade zero is then

$$\bar{f}^0(\bar{\phi}^0, \bar{\psi}^0) = \frac{\overline{\Delta p}_n}{\bar{r}_0^{1/2}} \frac{T(\bar{\chi}^n, \bar{\theta}_0)}{(\cos\bar{\chi}^n - \cos\bar{\theta}_0)} \exp(\mathrm{i}\bar{k}\bar{w}\bar{r}_0 + \mathrm{i}\bar{k}\bar{\delta}\bar{P}(\bar{r}_0, \bar{\theta}_0)) \tag{6.10}$$

where, in anticipation of work in a later section, we have introduced the superscript 0 to indicate that this field is produced by scattering from the trailing edge of blade 0. Here, $\bar{r}_0, \bar{\theta}_0$ are polar coordinates in $\bar{\phi}$–$\bar{\psi}$ space with the origin at the trailing edge of

blade 0, and $-\pi < \bar{\theta} < \pi$. The directivity function is $T(\bar{\chi}^n, \bar{\theta})/(\cos\bar{\chi}^n - \cos\bar{\theta})$, where

$$T(\bar{\chi}^n, \bar{\theta}) = \frac{\exp(\mathrm{i}3\pi/4)\cos\frac{1}{2}\bar{\chi}^n \sin\frac{1}{2}\bar{\theta}}{(2\pi\bar{k}^3\bar{w})^{1/2}(\bar{\beta}_\infty^{-2} - \bar{w}\cos\bar{\theta})}. \tag{6.11}$$

The directivity function has been written in this form for convenience in the following subsection. The amplitude of the cylindrical scattered field is weaker than the amplitude of the duct mode that generated it by a factor $\bar{k}^{-1/2}$, as can be seen from the denominator of (6.11), while the direct beams of (6.1) have the same scaling as the duct mode. The phase term $\bar{k}\bar{\delta}\bar{P}(\bar{r}, \bar{\theta})$ corresponds to the distortion experienced by the radiation as it propagates away from the trailing edge. Using (4.1) and noting that $\bar{F}(0) = 0$, we have

$$\bar{\delta}\bar{P}(\bar{r}, \bar{\theta}) = \bar{V}(\bar{\theta})\mathrm{Re}\{\exp(-\mathrm{i}\bar{\theta})\bar{\delta}\bar{F}(\bar{r}\mathrm{e}^{\mathrm{i}\bar{\theta}})\}, \tag{6.12}$$

where $\bar{V}(\theta)$ simply corresponds to $V(\theta)$ but with M_∞ replaced by $\bar{M}_\infty$ – see (3.2). It therefore follows that $\bar{\delta}\bar{P}$ is continuous across the blade wake.

Note that the directivity function is singular at $\bar{\theta}_0 = \mp\bar{\chi}_0$, corresponding to the boundaries of the downstream- and upstream-propagating beams which originate at the trailing edge of blade 0. This singularity arises from the coalescence of the saddle point with the pole at $\lambda = -\bar{w}\cos\bar{\chi}^n$ in the asymptotic expansion of (6.9), and is necessary in order for the scattered field to recover the amplitude scaling of the direct beams in these directions. A uniformly valid expression, as in Myers & Kerschen (1995, equation (3.51)), can be written down using the formula of Jones (1986, p. 720). This expression contains a complementary error function, which describes Fresnel regions of width $O(\bar{r}_0/\bar{k})^{1/2}$ along the directions $\bar{\theta}_0 = \pm\bar{\chi}^n$, surrounding one of the boundaries of the upper and lower beams of (6.1) – see figure 5. These Fresnel regions act to smooth out the step discontinuities in (6.1). The width of these Fresnel regions is small compared to the beam widths when $\bar{r}_0 \ll \bar{k}$. However, when $\bar{r}_0$ reaches $O(\bar{k})$, the Fresnel regions have spread to encompass the full width of the beams (region B in figure 5), and an alternative description is required. This alternative description is developed in § 6.4.

For a staggered cascade, the scattered field $\bar{f}^0$ from trailing edge 0 propagates directly to the far field for angles $-\pi + \bar{\alpha} < \bar{\theta}_0 < \bar{\alpha}$, while for angles $\bar{\alpha} < \bar{\theta}_0 < \pi/2$ the scattered field is reflected off the lower surface of blade 1 before propagating to the far field along the direction $-\bar{\theta}_0$ (see figure 4). As was argued at the end of § 2, the zero-normal-velocity boundary condition on each blade reduces simply to $\partial\bar{h}/\partial\bar{\psi} = 0$, and it therefore follows that the reflection of this direct field from trailing edge 0 by the lower surface of blade 1 can be accounted for by including an image source with modified potential $\bar{f}^0(\bar{\phi}^0, 2\bar{s} - \bar{\psi}^0)$. The reflected field $\bar{f}_r^0$ can be expressed in the form

$$\bar{f}_r^0(\bar{\phi}^0, \bar{\psi}^0) = [H(\bar{\theta}_{0r} + \bar{\alpha}) - H(\bar{\theta}_{0r} + \pi/2)]\frac{\overline{\Delta p}_n}{\bar{r}_{0r}^{1/2}}\frac{T(\bar{\chi}^n, \bar{\theta}_{0r})}{(\cos\bar{\chi}^n - \cos\bar{\theta}_{0r})} \times \exp(\mathrm{i}\bar{k}\bar{w}\bar{r}_{0r} + \mathrm{i}\bar{k}\bar{\delta}\bar{P}_r(\bar{\phi}^0, \bar{\psi}^0)), \tag{6.13}$$

where

$$\bar{r}_{0r} = [(\bar{\phi}^0)^2 + (2\bar{s} - \bar{\psi}^0)^2]^{1/2}, \quad \bar{\theta}_{0r} = -\cos^{-1}(\bar{\phi}^0/\bar{r}_{0r}), \tag{6.14}$$

and $-\pi/2 < \bar{\theta}_{0r} < -\bar{\alpha}$. The phase distortion along the reflected path,

$$\bar{k}\bar{\delta}\bar{P}_r(\bar{\phi}^0, \bar{\psi}^0) = \bar{k}\bar{\delta}\bar{V}(\bar{\theta}_{0r})[2\bar{\Delta}\sin(\bar{\theta}_{0r} + \bar{\alpha})/\bar{\beta}_\infty + \mathrm{Re}\{\exp(-\mathrm{i}\bar{\theta}_{0r})\bar{F}(\bar{\phi}^0 + \mathrm{i}\bar{\psi}^0)\}], \tag{6.15}$$

is calculated by applying (4.1) from trailing edge 0 to the point of reflection on blade 1, and then from that point to the observer location (points A, B and C in figure 4). Note that, for $\bar{\phi}^0 = O(1)$, the angles $\bar{\theta}_0$ and $\bar{\theta}_{0r}$ for the direct and reflected paths to the observer location are different, and it is $\bar{\theta}_{0r}$ that enters in the phase distortion $\bar{k}\bar{\delta}\bar{P}_r$.

6.3. *Scattering by the upper trailing edge*

Next we consider scattering of the duct mode of order n by the trailing edge of the upper blade. The upward-propagating component of the duct mode (5.9) reaches the trailing edge of the upper blade only when $\bar{\chi}^n < \bar{\alpha}$, as explained previously. The scattered field that is produced by this process is calculated in exactly the same way as has been described above. For definiteness, we again consider the duct mode in the passage between blades 0 and 1. The final result is

$$\bar{g}^1(\bar{\phi}^1, \bar{\psi}^1) = -\frac{\overline{\Delta p}_n}{\bar{r}_1^{1/2}} \frac{T(\bar{\chi}^n, \bar{\theta}_1) \exp(\mathrm{i}n\pi - \mathrm{i}\bar{k}^n \bar{d} + \mathrm{i}\bar{k}\bar{\delta}\mathscr{D}^n)}{(\cos\bar{\chi}^n - \cos\bar{\theta}_1)} \exp(\mathrm{i}\bar{k}\bar{w}\bar{r}_1 + \mathrm{i}\bar{k}\bar{\delta}\bar{P}(\bar{r}_1, \bar{\theta}_1)). \tag{6.16}$$

Here we have used the symbol $\bar{g}$ to distinguish the field produced by scattering of the duct mode at the upper trailing edge from the field $\bar{f}$ produced by scattering of the duct mode at the lower trailing edge. We have also introduced the superscript 1 to indicate that in this case the field is produced by scattering from trailing edge 1; $\bar{r}_1, \bar{\theta}_1$ are polar coordinates centred on the trailing edge of blade 1. The additional phase factor that appears in (6.16) is the phase of the incident duct mode at the location of the upper trailing edge, relative to the lower trailing edge. The first term in this additional phase factor arises from the anti-symmetry of the modes about the duct centreline for odd values of n, while the second term arises from the cascade stagger; these terms would also be present in uniform flow. The third term

$$\bar{k}\bar{\delta}\mathscr{D}^n = \bar{k}\bar{\delta}[\mathscr{F}^n(\bar{d}, \bar{s}) - \mathscr{F}^n(0, 0)] \tag{6.17}$$

is related to phase distortion of the duct mode by the non-uniform mean flow. Note that the weak mean flow variation has led to an $O(1)$ change in the phase of the duct mode at the upper trailing edge, relative to the lower trailing edge. The first minus sign on the right-hand side of (6.16) arises because in this case the pressure field of the incident and reflected plane waves exists in the region below, rather than above, the blade. The scattered field $\bar{g}^1$ is singular in the directions $\bar{\theta}_1 = \pm\bar{\chi}^n$. Again, this singularity can be removed by a uniformly valid asymptotic expansion involving complementary error functions, which serves to introduce Fresnel regions along the two remaining boundaries of the direct beams of (6.1).

The scattered field $\bar{f}^0$ from trailing edge 0 has one ray that propagates at the angle $\bar{\theta}_0 = \bar{\alpha}$ and therefore impinges on trailing edge 1, while the scattered field $\bar{g}^1$ from trailing edge 1 has one ray that propagates at the angle $\bar{\theta}_1 = -\pi + \bar{\alpha}$ and therefore impinges on trailing edge 0. These rays are re-scattered by the trailing edges that they impinge on, producing new rays that are subsequently re-scattered by the opposite trailing edge and this pattern continues indefinitely. The ray emanating from trailing edge 0 at angle $\bar{\theta}_0 = \pi/2$ undergoes a similar re-scattering process (see item iii in the discussion of the leading-edge rays in § 3). However, the amplitude of the re-scattered field is reduced by one power of $\bar{k}^{-1/2}$ at each stage in the infinite sequence of re-scattering processes. Hence, these re-scattering processes can be neglected in our high-frequency limit $\bar{k} \gg 1$.

Therefore, for $\bar{\chi}^n < \bar{\alpha}$ and $\bar{\phi} = O(1)$, the downstream field for radiation from a single blade passage consists of the direct beams (6.1) of amplitude $\bar{k}^{-2}$, supplemented by the scattered fields $\bar{f}^0$ and $\bar{g}^1$ of amplitude $\bar{k}^{-5/2}$. For a staggered cascade a portion of the scattered field $\bar{f}^0$ is reflected by blade 1 as described by (6.13), and this component also has amplitude $\bar{k}^{-5/2}$.

Next consider the case $\bar{\chi}^n > \bar{\alpha}$. Here, the upward-propagating component of the duct mode does not reach the trailing edge of the upper blade in the passage, as was explained in the derivation of (6.2). Hence, the contribution $\bar{g}^1$ does not arise in this case. For the scattered field $\bar{f}^0$ from the trailing edge of the lower blade, the singularity of the directivity function at $\bar{\theta}_0 = \bar{\chi}^n$ lies along the reflection boundary for the lower blade, which is then re-reflected by the upper blade, forming the downstream edge of the single beam of (6.2). When the expression (6.10) for $\bar{f}^0$ is replaced by a uniformly valid expression, the Fresnel region along $\bar{\theta}_0 = \bar{\chi}^n$ is reflected by the upper blade and acts to smooth the downstream edge of the direct beam (6.2). Therefore, for $\bar{\chi}^n > \bar{\alpha}$ and $\bar{\phi} = O(1)$, the downstream field for radiation from a single blade passage consists of the single downward-propagating beam (6.2) of amplitude $\bar{k}^{-2}$, supplemented by the scattered field $\bar{f}^0$ and its reflection (6.13) by the upper blade, both of amplitude $\bar{k}^{-5/2}$.

6.4. *Radiation from a single blade passage for* $\bar{r} \gg \bar{k}$

When the distance $\bar{r}$ along the duct-mode beams of (6.1) or (6.2) reaches $O(\bar{k})$, the Fresnel regions surrounding the edges of the beams have spread to encompass the whole width of the beams (region B in figure 5). As the field propagates farther downstream, the constant-amplitude beams disappear and the field exhibits the $\bar{r}^{-1/2}$ decay of a cylindrical wave field in all directions. In contrast to the near downstream field at $O(1)$ values of $\bar{\phi}$ where the dominant source is the direct duct-mode beams, the dominant source for the far-field radiation is the scattering of the duct mode by the trailing edges of the blades.

First consider the case $\bar{\chi}^n < \bar{\alpha}$. Here, the duct mode of order n is scattered by the trailing edges of both the lower and upper blades of the passage. The far downstream field produced by radiation of the order-n duct mode out of the passage between blades 0 and 1 is then given by the superposition of the scattered fields $\bar{f}^0$ and $\bar{g}^1$, plus the reflected field $\bar{f}^0_r$. Since we are considering the far field $\bar{r} \gg \bar{k}$, to the required order of accuracy we can set $\bar{\theta}_1 = \bar{\theta}_{0r} = \bar{\theta}_0$, $\bar{r}_1 = \bar{r}_0 - \bar{\Delta}\cos(\bar{\theta}_0 - \bar{\alpha})$, and $\bar{r}_{0r} = \bar{r}_0 - 2\bar{s}\sin\bar{\theta}_0$, where the $O(1)$ terms in $\bar{r}_1$ and $\bar{r}_{0r}$ need be retained only in the phase. In addition, noting that the mean flow variations in the vicinity of the cascade die off exponentially with distance downstream, we can replace the phase distortion by its asymptotic value $\bar{P}(\bar{r}, \bar{\theta}) = \bar{P}(\infty, \bar{\theta}) = \bar{V}(\bar{\theta})\mathrm{Re}[\exp(-\mathrm{i}\bar{\theta})\bar{F}(\infty)]$. Combining (6.10), (6.13) and (6.16), we then obtain

$$\bar{f}^0(\bar{\phi}^0, \bar{\psi}^0) + \bar{g}^1(\bar{\phi}^1, \bar{\psi}^1) + \bar{f}^0_r(\bar{\phi}^0, \bar{\psi}^0) = \frac{\overline{\Delta p}_n}{\bar{r}_0^{1/2}} \mathscr{T}_a(\bar{\chi}^n, \bar{\theta}_0) \exp(\mathrm{i}\bar{k}\bar{w}\bar{r}_0 + \mathrm{i}\bar{k}\bar{\delta}\bar{P}(\infty, \bar{\theta}_0)), \tag{6.18}$$

where

$$\begin{aligned}\mathscr{T}_a(\bar{\chi}^n, \bar{\theta}_0) = \frac{T(\bar{\chi}^n, \bar{\theta}_0)}{\cos\bar{\chi}^n - \cos\bar{\theta}_0} \Big[& 1 - \exp(-\mathrm{i}\bar{k}\bar{w}\bar{\Delta}[\cos(\bar{\theta}_0 - \bar{\alpha}) - \cos\bar{\chi}^n\cos\bar{\alpha}] \\ & + \mathrm{i}n\pi + \mathrm{i}\bar{k}\bar{\delta}\mathscr{D}^n) + [H(\bar{\theta}_{0r} + \bar{\alpha}) - H(\bar{\theta}_{0r} + \pi/2)]\exp(-\mathrm{i}\bar{k}\bar{w}2\bar{s}\sin\bar{\theta}_0 \\ & + \mathrm{i}\bar{k}\bar{\delta}2\bar{\Delta}\bar{V}(\bar{\theta}_0)\sin(\bar{\theta}_0 + \bar{\alpha})/\bar{\beta}_\infty) \Big]\end{aligned} \tag{6.19}$$

and we consider $-\pi + \bar{\alpha} < \bar{\theta}_0 < \bar{\alpha}$. The directivity pattern, $\mathscr{T}_a(\bar{\chi}^n, \bar{\theta}_0)$, for radiation from a single blade passage in the case $\bar{\chi}^n < \bar{\alpha}$, is seen to have the basic directivity pattern $T(\bar{\chi}^n, \bar{\theta})/(\cos\bar{\chi}^n - \cos\bar{\theta})$ for an isolated trailing edge, modified by interference between the waves from trailing edges 0 and 1, and by additional interference from the wave reflected off the lower surface of blade 1 for angles $-\pi/2 < \bar{\theta}_0 < -\bar{\alpha}$.

As already noted, $\bar{f}^0$ and $\bar{g}^1$ are singular when $\bar{\theta}_{0,1} = \pm\bar{\chi}^n$. For the near downstream region, these singularities are related to the edges of the beams of (6.1) and uniformly valid expansions are required in order to remove these non-uniformities. The situation is quite different in the far field $\bar{r}_0 \gg \bar{k}$. Here the constant-amplitude beams of (6.1) have disappeared, and a fixed observation point in the downstream region corresponds to nearly identical values for $\bar{\theta}_0$ and $\bar{\theta}_1$. We note that the singularities of $\bar{f}^0$ and $\bar{g}^1$ are of equal magnitude but opposite sign – this suggests that the singularities may cancel.

To examine this, first consider the behaviour $\mathscr{T}_a$ in the vicinity of the angles $\bar{\theta}_0 = \pm\bar{\chi}^n$ for the case $\bar{\delta} = 0$. These angles are outside the boundaries of the reflected field $\bar{f}^0_r$, so the second line of (6.19) can be ignored. Noting that $\bar{k}\bar{w}\sin\bar{\chi}^n = n\pi/\bar{s}$, it can be verified that the factor in the large square brackets in (6.19) vanishes for $\bar{\theta}_0 = \pm\bar{\chi}^n$. Hence, in the absence of mean flow distortions, the singularities of $\bar{f}^0$ and $\bar{g}^1$ cancel identically in the far field, leading to a cylindrically decaying field for all observation angles.

When $\bar{\delta} \neq 0$, however, the factor in the large square brackets in (6.19) vanishes when $\bar{\theta}_0 = \bar{\theta}_\pm$, say, which differ from $\pm\bar{\chi}^n$ by $O(\bar{\delta})$ amounts. The precise values of $\bar{\theta}_\pm$ can be found in a straightforward manner, and are

$$\left.\begin{aligned} \bar{\theta}_+ &= \bar{\alpha} - \cos^{-1}(\cos(\bar{\alpha} - \bar{\chi}^n) + \bar{\delta}\mathscr{D}^n/\bar{w}\bar{\Delta}), \\ \bar{\theta}_- &= \bar{\alpha} - \cos^{-1}(\cos(\bar{\alpha} + \bar{\chi}^n) + \bar{\delta}\mathscr{D}^n/\bar{w}\bar{\Delta}). \end{aligned}\right\} \tag{6.20}$$

(The argument of the first exponential function in (6.19) is equal to zero when $\bar{\theta}_0 = \bar{\theta}_+$, and is equal to $i n 2\pi$ when $\bar{\theta}_0 = \bar{\theta}_-$.) As it stands, (6.19) is therefore singular at $\bar{\theta}_0 = \pm\bar{\chi}^n$ for $\bar{\delta} \neq 0$. However, to the asymptotic order considered we are free to include corrections of relative size $O(\bar{\delta})$ in the amplitude of our acoustic fields, and it follows that we can replace the denominator in (6.19) by

$$\cos(\bar{\chi}^n + B) - \cos(\bar{\theta}_0 + A) \tag{6.21}$$

where $A = -(\bar{\theta}_+ + \bar{\theta}_-)/2$ and $B = -\bar{\chi}^n + (\bar{\theta}_+ - \bar{\theta}_-)/2$ are both $O(\bar{\delta})$. With this replacement, the expression (6.19) is non-singular for all values of the observer angle $\bar{\theta}_0$, and the far field decays as $\bar{r}_0^{-1/2}$ in all directions.

The cancellation of the singularities of $\bar{f}^0$ and $\bar{g}^1$ at distances $\bar{r} \gg \bar{k}$ is well known for the case $\bar{\delta} = 0$; this has been demonstrated by exact solutions of the scattering problem for two parallel plates. When $\bar{\delta} \neq 0$, the variations of the mean flow and the speed of sound have the effect of tilting the beams, by angles of size $O(\bar{\delta})$, away from the duct mode propagation directions $\pm\bar{\chi}^n$. The fact that the beams are tilted by differing amounts (i.e. in general $\theta_+ \neq -\theta_-$) of course corresponds to the asymmetry of the mean flow above and below each lifting airfoil.

Next consider the case $\bar{\chi}^n > \bar{\alpha}$. Here, the duct mode of order n does not reach the trailing edge of the upper blade in the passage, so that we have only the scattered field $\bar{f}^0$ from the trailing edge of the lower blade. The field $\bar{f}^0$ propagates directly to the far field for angles $\bar{\theta}_0 < \bar{\alpha}$, while for $\bar{\alpha} < \bar{\theta}_0 < \pi/2$ it is reflected off the lower surface of blade 1 and propagates to the far field along the direction $-\bar{\theta}_0$. Thus, the total field at large distances is the sum of the direct field $\bar{f}^0$ and the reflected field

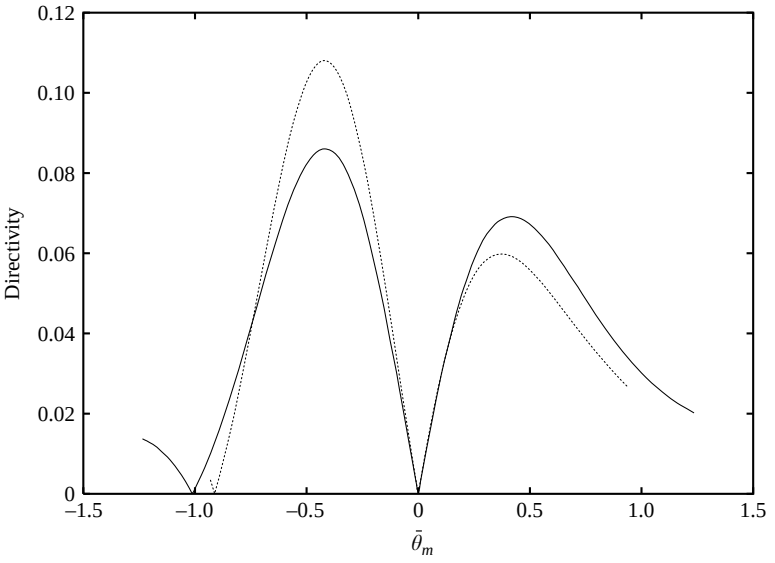

FIGURE 6. Plot of the far-field directivity pattern $|\mathscr{T}_a|$ for downstream radiation from a single blade passage, for $\delta = 0.3$ (solid line) and $\delta = 0$ (dotted line). Here we have $M_\infty = 0.6$, $k = 10$ $\Delta_*/b_* = \sqrt{2}$, $\sigma = \pi/2$, $\alpha_* = \pi/3 + \delta$, and the duct mode number is $n = 1$.

$\bar{f}_r^0$, which can be expressed in the form

$$\bar{f}^0(\bar{\phi}^0, \bar{\psi}^0) + \bar{f}_r^0(\bar{\phi}^0, \bar{\psi}^0) = \frac{\overline{\Delta p}_n}{\bar{r}_0^{1/2}} \mathscr{T}_b(\bar{\chi}^n, \bar{\theta}_0) \exp(\mathrm{i}\bar{k}\bar{w}\bar{r}_0 + \mathrm{i}\bar{k}\bar{\delta}\bar{P}(\infty, \bar{\theta}_0)), \tag{6.22}$$

where

$$\mathscr{T}_b(\bar{\chi}^n, \bar{\theta}_0) = \frac{T(\bar{\chi}^n, \bar{\theta}_0)}{\cos\bar{\chi}^n - \cos\bar{\theta}_0} \Big[1 - [H(\bar{\theta}_{0r} + \bar{\alpha}) - H(\bar{\theta}_{0r} + \pi/2)] \exp(-\mathrm{i}\bar{k}\bar{w}2\bar{s}\sin\bar{\theta}_0 + \mathrm{i}\bar{k}\bar{\delta}\bar{V}(\bar{\theta}_0)2\bar{\Delta}\sin(\bar{\theta}_0 + \bar{\alpha})/\bar{\beta}_\infty) \Big]. \tag{6.23}$$

The field $\bar{f}^0$ is singular in the direction $\bar{\theta}_0 = -\bar{\chi}^n$, as noted previously. The scattered field $\bar{f}^0$ is also singular in the direction $\bar{\theta}_0 = \bar{\chi}^n$, but this ray is reflected by blade 1 and is contained in $\bar{f}_r^0$ in (6.22). For $\bar{\delta} = 0$, the argument of the exponential in (6.23) takes the value $\mathrm{i}n2\pi$ when $\bar{\theta}_0 = -\bar{\chi}^n$, so that the singularity associated with the shadow boundary in the direct field $\bar{f}^0$ is cancelled by the corresponding singularity in the reflection of that direct field by blade 1, and $\mathscr{T}_b$ is non-singular. The effect of $\bar{\delta} \neq 0$ is to adjust the angle of the beam to $\bar{\theta}_0 = \bar{\theta}_r$, which differs from $-\bar{\chi}^n$ by an $O(\bar{\delta})$ amount, and which can easily be determined by setting the argument of the exponential in (6.23) to the value $\mathrm{i}n2\pi$. In order to remove the spurious singularity for the case $\bar{\delta} \neq 0$, we therefore once again introduce an $O(\bar{\delta})$ term into the amplitude, this time by replacing the denominator in (6.23) by

$$\cos\bar{\theta}_r - \cos\bar{\theta}_0. \tag{6.24}$$

Plots of the directivity pattern $|\mathscr{T}_a|$ of the downstream radiation from a single blade passage for the cases $\delta = 0$ and $\delta = 0.3$ are presented in figure 6. Results have been plotted for $-\bar{\alpha} < \bar{\theta}_0 < \bar{\alpha}$, which is the range of observer angles over which $\bar{f}_r^0$ does not contribute to (6.19). The $n = 1$ duct mode is considered; for the conditions chosen

we have the duct-mode angle $\bar{\chi}^n = 0.341$, while $\bar{\theta}_+ = 0.360$ and $\bar{\theta}_- = -0.326$. The presence of beams close to the directions $\bar{\theta}_\pm$ is clear in the figure. Note, however, that the direction of maximum amplitude of the beams is potentially displaced slightly from $\bar{\theta} = \bar{\theta}_\pm$ because, in a familiar way, the numerator of (6.19) has local extrema close to, but not precisely at, $\bar{\theta} = \bar{\theta}_\pm$. The lobular directivity pattern possesses a local $\bar{\theta}$ wavelength governed by the argument of the exponential function in (6.19), and it can be anticipated that the beam maxima lie within one quarter of this local wavelength about $\bar{\theta} = \bar{\theta}_\pm$. Note also that, while the shift in the location of the beams due to mean loading turns out to be relatively small for the case presented in figure 6, the effect on the directivity shape is quite significant. The introduction of mean loading has significantly augmented the beam above the horizontal (relative to the case $\delta = 0$), at the expense of the beam below the horizontal. This corresponds to the fact that in trailing-edge space the cascade is closer to being unstaggered for $\delta = 0.3$ than it is for $\delta = 0$ ($\bar{\alpha} = 1.2482$ and $\bar{\alpha} = 0.9457$ respectively), leading to a pattern which is more symmetric about $\bar{\theta}_0 = 0$.

6.5. *Radiation downstream of the cascade*

In §§6.1–6.4, we considered the radiation from a single blade passage. We now combine the fields from all the blade passages to determine the radiation downstream of the cascade. We again consider the radiation due to a single duct mode of order n. After the radiation for a single duct mode has been determined, the total downstream field is obtained by summing over the cut-on duct modes, $n = 0, 1, 2, \ldots, p$.

First consider the near downstream region (region A in figure 5). The distance normal to the back face of the cascade is $\bar{\phi}\sin\bar{\alpha} - \bar{\psi}\cos\bar{\alpha}$. We define the near downstream region as distances small compared to $\bar{k}$. For the near downstream region, we showed in §6.1 that the radiation from a single blade passage consists of two constant-width beams (6.1) propagating in the directions $\pm\bar{\chi}^n$ when $\bar{\chi}^n < \bar{\alpha}$, or a single beam (6.2) propagating in the direction $-\bar{\chi}^n$ when $\bar{\chi}^n > \bar{\alpha}$. The radiation from the cascade then consists of an infinite number of parallel beams, propagating in these same directions. From the basic periodicity properties for the cascade, the field which emanates from passage m (between blades m and $m+1$) is identical to that from passage 0, except for the introduction of a phase factor $\exp(\mathrm{i}m\bar{\sigma}')$, and a shift of the origin to the trailing edge of blade m. Here $\bar{\sigma}' = \sigma + \bar{k}\bar{M}_\infty^2\bar{d}/\bar{\beta}_\infty^2$, where $\bar{d} = \bar{\Delta}\cos\bar{\alpha}$.

For $\bar{\chi}^n < \bar{\alpha}$, the downward-propagating beams of width $\bar{\Delta}\sin(\bar{\alpha} + \bar{\chi}^n)$ cover all of downstream $\bar{\phi}$–$\bar{\psi}$ space, and the upward-propagating beams of width $\bar{\Delta}\sin(\bar{\alpha} - \bar{\chi}^n)$ cover the full downstream space as well. A given point $(\bar{\phi}, \bar{\psi})$ lies within only one downward-propagating beam and one upward-propagating beam. The value of the modified potential $\bar{h}(\bar{\phi}, \bar{\psi})$ can then be found by using simple geometry to determine the passages from which the relevant downward- and upward-propagating beams emanated, and employing the expressions for these beams given earlier.

For $\bar{\chi}^n > \bar{\alpha}$, the upward-propagating beams are blocked by the trailing edge of the adjacent upper blade, and the downstream field for the cascade consists of an infinite number of parallel downward-propagating beams of width $2\bar{\Delta}\sin\bar{\alpha}\cos\bar{\chi}^n$, separated by shadow regions of width $\bar{\Delta}\sin(\bar{\chi}^n - \bar{\alpha})$. Hence, for this case, a given downstream point $(\bar{\phi}, \bar{\psi})$ may lie in a beam or in a shadow region. Again, the value of the modified potential can be found from simple geometry combined with (6.2) and the periodicity property for the downstream field.

The scattered cylindrical fields from each trailing edge must be added to the primary field consisting of the beams discussed above. These scattered fields were calculated

in §§6.2, 6.3. The amplitudes of the scattered fields are smaller than that of the primary field by a factor $\bar{k}^{-1/2}$. Hence, the scattered fields are relatively unimportant when considering points that lie within a beam of the primary field. The beams of the primary field cover all of downstream space when $\bar{\chi}^n < \bar{\alpha}$, and we note that this applies to well cut-on duct modes. For $\bar{\chi}^n > \bar{\alpha}$, a field point may lie in one of the shadow regions; in this case the value of the modified potential is determined by the scattered cylindrical fields. For near downstream locations, the nearby trailing edges make the most important contributions to the scattered field, so that this component is calculated most conveniently from the summation over blade index m in (6.25).

For far downstream distances, corresponding to $\bar{\phi}\sin\bar{\alpha} - \bar{\psi}\cos\bar{\alpha} \gg \bar{k}$, a quite different picture emerges. Here (downstream of B in figure 5) the dominant contribution to the field comes from the scattering of the duct modes by the trailing edges. Expressions for the far downstream field produced by radiation of the duct mode of order n from a single blade passage were developed in §6.4, by properly combining the effects of adjacent trailing edges. In constructing these expressions, care was taken to cancel the singularities at $\bar{\theta}_m = \pm\bar{\chi}^n$ in the directivity pattern for scattering from a single trailing edge. These singularities arose from the neglect of the finite width of the duct-mode beam in the local analysis of §§6.2, 6.3, and are not relevant to the far-field region. The total field downstream of the cascade, produced by impingement of the cut-on duct mode of order n, can then be written in the general form

$$\bar{h}(\bar{\phi}, \bar{\psi}) = \overline{\Delta p}_n \sum_{m=-\infty}^{\infty} \frac{\mathscr{T}(\bar{\chi}^n, \bar{\theta}_m)}{\bar{r}_m^{1/2}} \exp(\mathrm{i}\bar{k}\bar{w}\bar{r}_m + \mathrm{i}\bar{k}\bar{\delta}\bar{P}(\infty, \bar{\theta}_m) + \mathrm{i}m\bar{\sigma}'). \tag{6.25}$$

Here

$$\bar{r}_m = [(\bar{\phi} - m\bar{d})^2 + (\bar{\psi} - m\bar{s})^2]^{1/2}, \quad \bar{\theta}_m = \tan^{-1}[(\bar{\psi} - m\bar{s})/(\bar{\phi} - m\bar{d})] \tag{6.26}$$

are polar coordinates with origin at the trailing edge of blade m, and $\bar{k}\bar{\delta}\bar{P}(\infty, \bar{\theta}_m)$ is the phase distortion induced by the mean flow variations in the vicinity of the cascade, for propagation from the trailing edge of blade m to infinity along the direction $\bar{\theta}_m$. Note that the contribution from passage m is shifted by the phase factor $\exp(\mathrm{i}m\bar{\sigma}')$, reflecting the periodic nature of the cascade field.

The function $\mathscr{T}(\bar{\chi}^n, \bar{\theta}_m)$ is the directivity pattern for radiation from a single blade passage, which was determined in §6.4. When $\bar{\chi}^n < \bar{\alpha}$, the directivity function is $\mathscr{T}_a$, modified according to (6.21), while for $\bar{\chi}^n > \bar{\alpha}$ the directivity function is $\mathscr{T}_b$, modified according to (6.24).

Equation (6.25) contains the direct field from each trailing edge produced by the scattering of the incident duct mode, and the reflection of each direct field by the adjacent upper blade in the case of a staggered cascade. The direct radiation from a single trailing edge (and its reflection by the adjacent upper blade for a staggered cascade) is $O(kw)^{-5/2}$; this can be seen from (6.11) and from the fact that $\overline{\Delta p}_n = O(1/kw)$. As well as being reflected by an adjacent blade, the direct field from each trailing edge will also be re-scattered by the other trailing edges, in exactly the same way as was described in (I) for the leading-edge field. These re-scattered components could easily be included in our analysis, in almost exactly the same way as was done in (I), but their inclusion here would only complicate the results, and certainly adds no new insight, and we therefore choose to omit them. This is an entirely consistent approach, since the re-scattered components are at most $O(kw)^{-3}$, and are therefore smaller than the direct field. In effect, we therefore include the first two terms in the phase (of $O(k)$ and $O(k\delta)$, respectively) and now just the first term

in the amplitude of the downstream radiation. Note, however, that the first term in the amplitude contains components that are proportional to $k\delta$, so that the amplitude has been modified by $O(1)$ amounts due to the effects of mean loading.

While the infinite sum over blade index in (6.25) is convenient for calculating the scattered field at close distances, it becomes poorly convergent far downstream where a large number of blades are approximately equidistant from the observation point. The field far downstream is most easily calculated by converting the infinite sum of cylindrically decaying waves into a sum of plane-wave radiation modes. This conversion is completed using Poisson summation in exactly the same way as described in (I) for the upstream radiation, and which is indeed very similar to the method described in § 4.2 of this paper for the field between the blades. We will therefore state just the final result here; the modified unsteady potential in the far field downstream of the cascade is

$$\bar{h}(\bar{\phi}, \bar{\psi}) = \overline{\Delta p}_n \sum_{m=-\bar{r}}^{\bar{q}} A_{mn} \exp(-\mathrm{i}\sigma^m \bar{x}_*/b_* - \mathrm{i}\eta^m \bar{\beta}_\infty \bar{y}_*/b_*), \tag{6.27}$$

where the index m now corresponds to the mode order for the radiation modes in the downstream region, rather than the blade index as in (6.25). The modal wavenumbers are

$$\left.\begin{aligned} \sigma^m &= \left[(2m\pi - \bar{\sigma}')\cos\bar{\alpha} - [\bar{\Delta}^2\bar{k}^2\bar{w}^2 - (2m\pi - \bar{\sigma}')^2]^{1/2}\sin\bar{\alpha}\right]/\bar{\Delta}, \\ \eta^m &= \left[(2m\pi - \bar{\sigma}')\sin\bar{\alpha} + [\bar{\Delta}^2\bar{k}^2\bar{w}^2 - (2m\pi - \bar{\sigma}')^2]^{1/2}\cos\bar{\alpha}\right]/\bar{\Delta}. \end{aligned}\right\} \tag{6.28}$$

The transmission coefficients A_{mn} are given by

$$A_{mn} = \frac{(2\pi\bar{k}\bar{w})^{1/2}\exp(\mathrm{i}\pi/4)\mathscr{T}\left(\bar{\chi}^n, \bar{\theta}^s_m\right)}{[\bar{\Delta}^2\bar{k}^2\bar{w}^2 - (2m\pi - \bar{\sigma}')^2]^{1/2}} \exp(-\mathrm{i}\sigma^m \mathrm{Re}[\bar{\delta}\bar{F}(\infty)] - \mathrm{i}\eta^m \mathrm{Im}[\bar{\delta}\bar{F}(\infty)])\Big], \tag{6.29}$$

where

$$\bar{\theta}^s_m = \tan^{-1}(\eta^m/\sigma^m) \quad \text{with} \quad -\pi + \bar{\alpha} < \bar{\theta}^s_m < \bar{\alpha} \tag{6.30}$$

corresponds to the propagation direction of the downstream mode. The phase term in (6.29) arises simply from writing down the far-field form of $\bar{\phi}$ and $\bar{\psi}$. Equation (6.27) makes it clear that each of the cut-on duct modes (labelled n) in the blade passages is scattered into each of the cut-on radiation modes downstream (labelled $m = -\bar{r}, \ldots, \bar{q}$), with an amplitude equal to $\overline{\Delta p}_n A_{mn}$, emphasizing the fact that it is the pressure jump at the trailing edge associated with each duct mode which generates the radiation far downstream.

Only a finite number of the radiation modes are cut on, and therefore need to be included in the far field, and the integers $-\bar{r}$ and $\bar{q}$ are such that these cut-on modes satisfy $-\bar{r} \leqslant m \leqslant \bar{q}$. For the radiation mode with mode number m to be cut on downstream of the cascade we require that $|2m\pi - \bar{\sigma}'| < \bar{\Delta}\bar{k}\bar{w}$, while the condition for radiation modes to be cut on upstream is that $|2m\pi - \sigma'| < \Delta k w$, and it is then easy to see that the numbers of modes cut on ahead of and behind the cascade may be different. It is well-known that the swirl induced by a blade row affects the number of modes which are cut on. In the present analysis we have identified precisely the role of the circulation Γ in altering the periodicity properties of the effective sources: upstream the sources are located in ϕ–ψ space with stagger α, spacing Δ and modified inter-blade phase angle σ', while for the downstream flow they are located in $\bar{\phi}$–$\bar{\psi}$ space with different stagger $\bar{\alpha}$, spacing $\bar{\Delta}$ and modified inter-blade phase angle $\bar{\sigma}'$. When $\delta = 0$ the upstream and downstream parameters are identical, and the mode

counts upstream and downstream become identical as well. The expression (6.29) is singular whenever $\bar{\Delta}^2\bar{k}^2\bar{w}^2 = (2m\pi - \bar{\sigma}')^2$, and it is easy to see that this is the cut-off condition for the radiation modes and corresponds to the two critical cases $\bar{\theta}^s_m = \bar{\alpha}$ and $\bar{\theta}^s_m = -\pi + \bar{\alpha}$, in which the modal propagation direction is aligned along the back face of the cascade and the radiation does not propagate to the far field.

We note here that there is a clear connection between the wavenumbers in our two-dimensional cascade model and the azimuthal order of the corresponding cylindrical duct modes in an annular cascade model. If one considers the incident gust as having been generated upstream by a rotating blade row of B blades, and if we suppose that the cascade is part of a stator row of V vanes, then it is easy to see that the inter-blade phase angle, σ, is just $2\pi NB/V$ for integer N. When we consider the scattered field, (6.27), and resolve the wavenumbers in the direction along the face of the cascade, we find that this leads to an azimuthal dependence $\exp(\mathrm{i}\bar{m}\theta)$, where the order $\bar{m}$ for each outgoing radiation mode is given by $\bar{m} = NB - mV$, where m is the cascade mode index. This is exactly the famous Tyler & Sofrin (1962) result.

In order to demonstrate the possible effects of varying the mean loading on the downstream unsteady flow, we consider a specific case in which $M_\infty = 0.6$, $k = 10$, $\Delta_*/b_* = \sqrt{2}$, and $\alpha_* = \pi/3 + \delta$. This corresponds to introducing mean loading by rotating each blade in the cascade in the clockwise direction about its leading edge, while holding the upstream mean flow fixed. When mean loading is introduced in this way, the leading-edge spacing and cascade stagger angle in ϕ–ψ space take on the values $\Delta = 1.2083$ and $\alpha = 0.9457$, independent of δ. We consider values of mean loading in the range $0 \leqslant \delta \leqslant 0.3$. Using the method described in § 5.1, for $\delta = 0.3$ we have $\bar{\delta} = 0.0561$ and $\bar{U}_\infty = 0.8602U_\infty$, leading to the downstream reduced frequency $\bar{k} = 11.6252$, while $\bar{M}_\infty = 0.5114$, $\bar{\rho}_\infty = 1.0475\rho_\infty$, and finally $\bar{\Delta} = 1.2316$ and $\bar{\alpha} = 1.2482$. Comparing the values of δ and $\bar{\delta}$, it can be seen that most of the mean flow turning occurs near the upstream side of the cascade, as a consequence of the Kutta condition.

In figure 7 we choose $\delta = 0.3$, and vary the inter-blade phase angle σ, which means that the cascade parameters in trailing-edge space will remain fixed, but that the propagation angles of the downstream modes, $\bar{\theta}^s_m$, will continuously rotate as σ is varied. Two points are apparent from figure 7. First, the nulls in $|A_{02}|$ correspond to the case in which the mode propagation angle $\bar{\theta}^s_0$ passes through zero, so that from (6.11) the directivity here is exactly zero. Indeed, provided that $\bar{\chi}^n \neq 0$ (i.e. we are not considering the scattering of the plane-wave duct mode), then the amplitude of a downstream radiation mode which propagates parallel to the far-downstream steady flow is necessarily zero. This remains true even if multiple re-scattering of the trailing-edge field were included, thanks to the $\sin\frac{1}{2}\bar{\theta}$ directivity from any scattering by a trailing edge. In the case $\bar{\chi}^n = 0$ (not shown in figure 7), the direction of the downstream beam is close to $\bar{\theta} = 0$ and the $\sin\frac{1}{2}\bar{\theta}$ factor is cancelled by the denominator in (6.19) to yield a finite and non-zero result for the amplitude. The second point to be made from figure 7 is that the maximum in $|A_{12}|$ corresponds to the coincidence between $\bar{\theta}^s_1$ and the beam direction $\bar{\theta}_-$ discussed in § 6.4. This demonstrates how significantly larger modal amplitudes are to be expected when the mode propagation direction is close to one of the beam directions $\bar{\theta}_\pm$.

In figure 8 we set $\sigma = \pi/2$ to fix the upstream gust characteristics, and vary δ from 0 up to 0.3. For $\delta = 0$ the cut-on mode numbers downstream are $0 \leqslant m \leqslant 2$, while for $\delta = 0.3$ we have $-1 \leqslant m \leqslant 2$, so that one additional mode has become cut-on downstream due to the mean loading. Because of the way in which the mean loading is being varied, it follows that upstream the cut-on modes remain as $0 \leqslant m \leqslant 2$

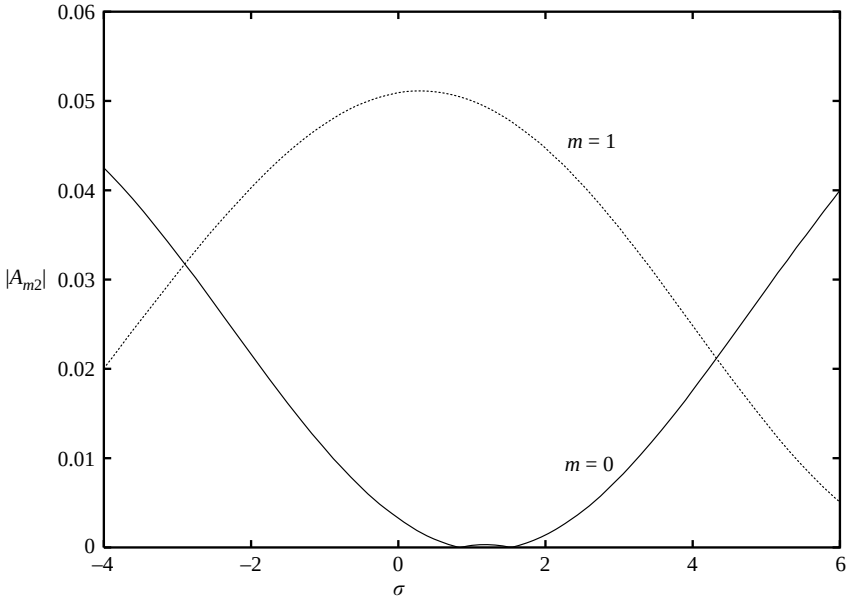

FIGURE 7. Plot of the modal amplitudes $|A_{02}|$ (solid line) $|A_{12}|$ (dotted line) for $\delta = 0.3$ and varying inter-blade phase angle σ, all other parameters as in figure 6.

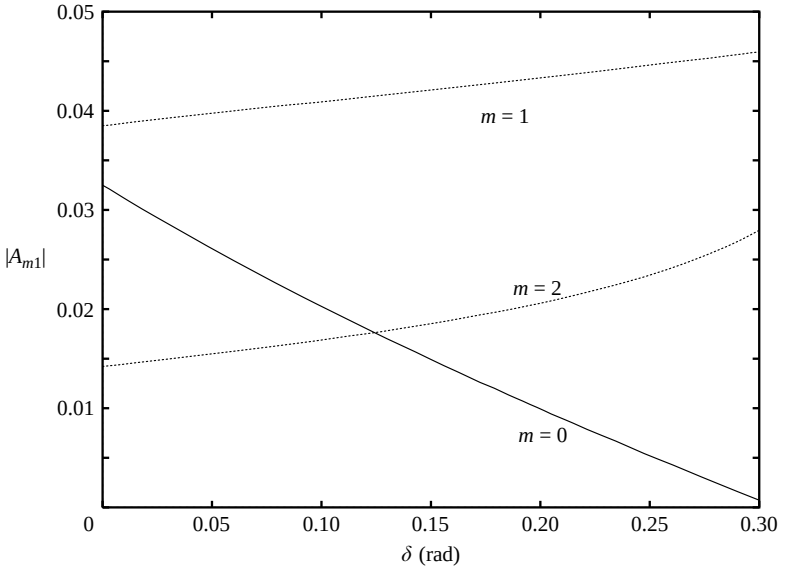

FIGURE 8. Variation in $|A_{m1}|$ as angle-of-attack to the upstream flow, δ, is increased for $m = 0, 1, 2$, and $\sigma = \pi/2$, other conditions as in figure 6.

throughout, confirming the point made earlier that the flow turning can in this case cut on additional modes downstream.

We can see in figure 8 that increasing the mean loading has a significant effect on the downstream modal amplitudes. The values of $|A_{11}|$ and $|A_{21}|$ increase with δ, while $|A_{01}|$ decreases. The null in $|A_{01}|$ just beyond $\delta = 0.3$ corresponds to the $m = 0$ downstream mode becoming aligned with the downstream flow. The changes observed

with varying δ are due to the variation of all the downstream flow parameters, but by looking at the numbers at the beginning of this paragraph it becomes clear that it is the variation in the effective stagger $\bar{\alpha}$ which is having the biggest effect on the radiation in this case. Another point, not apparent in the amplitude plots shown here, is the fact that the additional phase distortion experienced by a given mode as it propagates downstream from the cascade, as expressed by the term $\bar{\delta}\bar{F}(\infty)$ in (6.29), will typically be small, due to the fact that the downstream flow will tend to be almost aligned with the blade trailing edges (i.e. $\bar{\delta}$ is numerically much smaller than δ).

In summary, the results shown in this subsection emphasize once again, we believe, the very significant effect that mean loading can have on the unsteady flow through a cascade.

7. Concluding remarks

In this paper we have investigated the acoustic field generated by the interaction between a cascade of airfoils at non-zero angle of attack and unsteady upstream disturbances, with particular reference to the fields in the blade passages and downstream of the cascade. For the high-frequency limit considered here, the noise generation is concentrated in regions of size $O(k^{-1})$ around each leading edge, and this interaction has already been analysed in (I). In this paper our chief concern has been with the way in which this sound interacts with both the blades and the non-uniform steady flow. In particular, we have been able to analyse the complicated way in which the multiply reflected ray paths experience phase distortions as they propagate downstream through the non-uniform flow between the blades. This has led to an analytical representation for the modified duct modes; since the non-uniform-flow correction terms in these results are all $O(1)$ in our preferred limit, the effects of the blade incidence must be particularly significant.

At $O(1)$ distances downstream of the cascade, the field is dominated by the direct radiation of duct-mode beams out of the back of the cascade, and explicit expressions for the field in this region, including the $O(1)$ phase distortions due to non-uniform mean flow effects, have been presented. These expressions could be utilized to consider interactions with downstream obstacles, such as additional blade rows, struts, pylons or the like. In situations where no obstacles are present downstream, propagation to the far field is of interest. At distances of $O(k)$ along the ray path, the Fresnel regions along the edges of the duct-mode beams have spread to encompass the full width of the beams, and a different representation is required. We have shown how the far-field radiation modes can be recovered by a suitable coordinate transformation, and indeed the modal cut-off conditions are reproduced exactly, and not just to $O(\delta)$ – since cascade prediction schemes tend to be particularly sensitive near cut-off, we believe that this is an important feature. We have identified a strong beaming effect, when the downstream radiation modes propagate close to the corresponding duct-mode directions corrected for the effects of non-uniform flow. Although our results are non-singular when the radiation modes propagate along the beam directions referred to above, our expressions for the downstream modal amplitudes are singular at cut-off (as are the upstream modal amplitudes in paper (I)). Recently, Evers & Peake (2002) have shown that these singularities can be smoothed out upstream, to produce uniformly valid modal amplitudes for non-uniform flow (this has been completed by introducing corrections into Peake & Kerschen's (1995) uniformly valid solution for uniform flow), and it can be anticipated that exactly the same approach would be successful downstream as well.

We note that while the solution presented here has been completed for flat-plate airfoils at incidence, similar results for cambered blades with finite thickness can also be found. The general structure of the downstream field (Fresnel regions and beams) is certainly found, while qualitatively the modal structure between the blades is also recovered. However, expressions for the duct modes with camber and thickness included are less compact than those given in § 4. This is because the imaginary part of the steady disturbance potential, Im[F], on the blade surface will depend on the detailed thickness and camber distributions of the blades, so that the phase distortion experienced by the bouncing ray shown in figure 3, and given in equation (4.2), will depend on the blade thickness and camber at each bounce. The relatively simple expressions for $\wp_{1-4}$ given in § 4.1 therefore become significantly more complicated. The point about the downstream duct modes which are close to cut-off being turned round by the non-uniform flow also pertains when thickness and camber are included, and presumably the area variation of the blade passage associated with the thickness and camber could make such a cut-off more likely.

Finally with regard to the inclusion of camber and thickness, Atassi (1984) has shown that in incompressible flow the unsteady lift on a cambered, thick airfoil at incidence can be written as a linear combination of contributions from the camber and thickness distributions and the mean loading considered separately. This result does not appear to carry over to our compressible case, however. Consider the work of Myers & Kerschen (1997) for a cambered airfoil with zero thickness, say incidence angle $O(\delta_i)$ and camber angle $O(\delta_c)$. In their equation (5.7) an expression is given for the so-called leading-edge transition field on the blade surface. This can be seen to contain the factor $\exp(\mathrm{i}k\sigma_l)$, where $\sigma_l = wr + \sigma_{1l}$ and σ_{1l} is given in their equation (4.3a). (Note that their equation (4.3a) has a typographical error – it should read $V(\theta)$, so that σ_{1l} does not vanish on the airfoil upper surface $\theta = 0$.) The factor $\exp(\mathrm{i}k\sigma_{1l})$ corresponds to the phase distortion experienced by the field from the leading edge as it propagates along the curved blade surface, and it follows that $\exp(\mathrm{i}k\sigma_{1l})$ is of the form

$$\exp(\mathrm{i}[O(kw\delta_i) + O(kw\delta_c)]). \tag{7.1}$$

Since Myers & Kerschen use the preferred limit $k\delta_{i,c} = O(1)$, it is clear that the exponential (7.1) cannot be expanded for small argument, and the field on the blade is nonlinearly dependent on δ_i and δ_c. Of course, if we were now to keep $k\delta_{i,c} = O(1)$, but take the low-Mach-number limit (in the two-dimensional case by sending $w \to 0$) then the exponential in (7.1) could be expanded, and Atassi's result of a field which is linear in $\delta_{i,c}$ would be realised.

The authors gratefully acknowledge the financial support provided by the Nuffield Foundation (N. P.) and NASA under grant NAG3-1442 (E. J. K).

REFERENCES

Abdelhamid, Y. A. & Atassi, H. M. 2000 Effects of blade shape and loading on the acoustic radiation of a cascade. *AIAA Paper* 2000-2093-CP.

Atassi, H. M 1984 The Sears problem for a lifting airfoil revisited-new results. *J. Fluid Mech.* **141**, 109–122.

Atassi, H. M., Subramaniam, S. & Scott, J. R. 1990 Acoustic radiation from lifting airfoils in compressible subsonic flow. *AIAA Paper* 90-3911.

Davies, B. 1985 *Integral Transforms and Their Applications*. Springer.

Evers, I. & Peake, N. 2002 On sound generation by the interaction between turbulence and a cascade of airfoils with non-uniform mean flow. *J. Fluid Mech.* **463**, 25–52.

Goldstein, M. E. 1978 Unsteady vortical and entropic disturbances of potential flows round arbitrary obstacles. *J. Fluid Mech.* **89**, 433–468.

Jones, D. S. 1966 *Generalised Functions.* McGraw-Hill.

Jones, D. S. 1986 *Acoustic and Electromagnetic Waves.* Oxford University Press.

Jones, D. S. 1994 *Methods in Electromagnetic Wave Propagation.* Oxford University Press.

Kerschen, E. J. & Balsa, T. F. 1981 Transformation of the equation governing disturbances of a two-dimensional compressible flow. *AIAA J.* **19**, 1367–1370.

Kerschen, E. J. & Myers, M. R. 1986 Perfect gas effects in compressible rapid distortion theory. *AIAA J.* **25**, 504–507.

Koch, W. 1971 On the transmission of sound waves through a blade row. *J. Sound Vib.* **18**, 111–128.

Myers, M. R. & Kerschen, E. J. 1995 Influence of incidence angle on sound generation by airfoils interacting with high-frequency gusts. *J. Fluid Mech.* **292**, 271–304.

Myers, M. R. & Kerschen, E. J. 1997 Influence of camber on sound generation by airfoils interacting with high-frequency gusts. *J. Fluid Mech.* **353**, 221–259.

Peake, N. 1992 The interaction between a high-frequency gust and a blade row. *J. Fluid Mech.* **241**, 261–289.

Peake, N. 1993 The scattering of vorticity waves by an infinite cascade of flat plates in subsonic flow. *Wave Motion* **18**, 255–271.

Peake, N. & Kerschen, E. J. 1995 A uniform asymptotic approximation for high-frequency unsteady cascade flow. *Proc. R. Soc. Lond.* A **449**, 177–186.

Peake, N. & Kerschen, E. J. 1997 Influence of mean loading on noise generated by the interaction of gusts with a flat-plate cascade: upstream radiation. *J. Fluid Mech.* **347**, 315–346 (referred to herein as (I)).

Robinson, A. & Laurmann, J. A. 1956 *Wing Theory.* Cambridge University Press.

Tyler, J. M. & Sofrin, T. G. 1962 Axial flow compressor noise studies. *SAE Trans.* **70**, 309–332.

Verdon, J. M. 1993 Review of unsteady aerodynamic methods for turbomachinery aeroelastic and aeroacoustic applications. *AIAA J.* **31**, 235–250.

Yee, H. Y., Felsen, L. B. & Keller, J. B. 1968 Ray theory of reflection from the open end of a waveguide. *SIAM J. Appl. Maths* **16**, 268–300.